Neoproterozoic basement history of Wrangel Island and Arctic Chukotka: integrated insights from zircon U–Pb, O and Hf isotopic studies

ERIC S. GOTTLIEB[1]*, VICTORIA PEASE[2], ELIZABETH L. MILLER[1] & VYACHESLAV V. AKININ[3]

[1]*Stanford University, Geological Sciences, 450 Serra Mall, Building 320, Stanford, California 94305, USA*

[2]*Department of Geological Sciences, PetroTectonics Centre, Stockholm University, 106 91 Stockholm, Sweden*

[3]*North-East Interdisciplinary Scientific Research Institute, Far East Branch–Russian Academy of Sciences, 685000 Magadan, 16 Portovaya Street, Magadan, Russia*

**Correspondence: esgeo@stanford.edu*

Abstract: The pre-Cenozoic kinematic and tectonic history of the Arctic Alaska Chukotka (AAC) terrane is not well known. The difficulties in assessing the history of the AAC terrane are predominantly due to a lack of comprehensive knowledge about the composition and age of its basement. During the Mesozoic, the AAC terrane was involved in crustal shortening, followed by magmatism and extension with localized high-grade metamorphism and partial melting, all of which obscured its pre-orogenic geological relationships. New zircon geochronology and isotope geochemistry results from Wrangel Island and western Chukotka basement rocks establish and strengthen intra- and inter-terrane lithological and tectonic correlations of the AAC terrane. Zircon U–Pb ages of five granitic and one volcanic sample from greenschist facies rocks on Wrangel Island range between 620 ± 6 and 711 ± 4 Ma, whereas two samples from the migmatitic basement of the Velitkenay massif near the Arctic coast of Chukotka yield 612 ± 7 and 661 ± 11 Ma ages. The age spectrum (0.95–2.0 Ga with a peak at 1.1 Ga and minor 2.5–2.7 Ga) and trace element geochemistry of inherited detrital zircons in a 703 ± 5 Ma granodiorite on Wrangel Island suggests a Grenville–Sveconorwegian provenance for metasedimentary strata in the Wrangel Complex basement and correlates with the detrital zircon spectra of strata from Arctic Alaska and Pearya. Temporal patterns of zircon inheritance and O–Hf isotopes are consistent with Cryogenian–Ediacaran AAC magmatism in a peripheral/external orogenic setting (i.e. a fringing arc on rifted continental margin crust).

Supplementary material: Secondary ion mass spectrometry (SIMS) U–Pb zircon geochronology data, SIMS zircon $^{18}O/^{16}O$ isotopic data, laser ablation inductively coupled mass spectrometry zircon Lu–Hf isotopic data and zircon cathodoluminescence images are available at https://doi.org/10.6084/m9.figshare.c.3741314

The Arctic Alaska Chukotka (AAC) terrane, forming the Alaskan–Russian margin of the modern Arctic Ocean basin, includes Arctic Alaska, Chukotka and the Chukchi Sea Shelf, and portions of the East Siberian, Beaufort and Bering Sea shelves (Fig. 1). The AAC terrane's enigmatic role in the plate tectonic evolution of the Arctic region is complicated by multiple episodes of deformation and magmatism (e.g. Miller *et al.* this volume, in press *a*) and thus determining its early geological history poses major challenges. Understanding this history is essential to elucidating palaeotectonic associations of the AAC terrane with other basement complexes in the circum-Arctic realm.

The AAC terrane contains numerous exposures of Neoproterozoic metamorphic and igneous basement overlain by a Palaeozoic and Mesozoic sedimentary cover sequence (e.g. Cecile *et al.* 1991; Patrick & McClelland 1995; Amato *et al.* 2009, 2014; Miller *et al.* 2010; Pease *et al.* 2014; Till *et al.* 2014*a*; Akinin *et al.* 2015). This paper focuses on the geochronology and isotope geochemistry of Neoproterozoic basement rocks from two localities (western Chukotka and Wrangel Island; Figs 1 & 2) that are exposed *c.* 250 km apart in the central part of the AAC terrane. Although in close proximity relative to the total size of the AAC terrane (Fig. 1), these exposures have never previously

From: Pease, V. & Coakley, B. (eds) *Circum-Arctic Lithosphere Evolution*. Geological Society, London, Special Publications, **460**, https://doi.org/10.1144/SP460.11

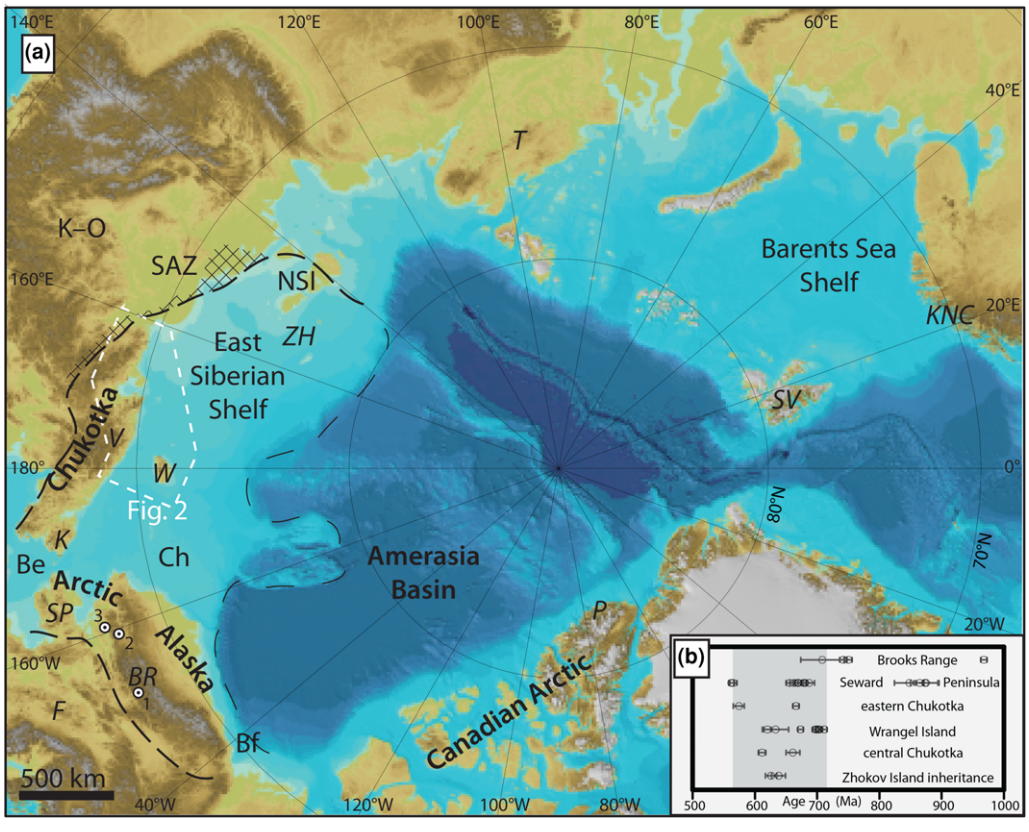

Fig. 1. (**a**) Circum-Arctic topography and bathymetry in polar projected image (Jakobsson *et al.* 2012) showing the location of the AAC terrane, delineated along its northern flank by the shelf to slope break (light dashed line) and across continental and marine shelves by the geological and geophysical constraints discussed in text (bold dashed line). Dashed white polygon shows the location of Figure 2. AAC regions: BR, Brooks Range; K, Koolen Dome; NSI, New Siberian Islands; SP, Seward Peninsula; V, Velitkenay massif; W, Wrangel Island; ZH, Zhokov Island of DeLong archipelago. Continental shelf areas: Be, Bering Sea Shelf; Bf, Beaufort Sea Shelf; Ch, Chukchi Sea Shelf. Numbered locations in Brooks Range: 1, Ernie Lake; 2, Mt Angayukaqsraq; 3, Kallarichuk Hills. Other regions referred to in text: F, Farewell Terrane; KNC, Kalak Nappe Complex; K–O, Kolyma–Omolon block; P, Pearya terrane; SAZ, South Anyui Zone (cross-hatched area, Amato *et al.* 2015); SV, Svalbard; T, Central Taimyr. Italicized labels indicate areas with geochronology data relevant to parts of this study. (**b**) Age range of magmatism ($\pm$2s error bars) based on zircon U–Pb ages reported in various parts of the AAC, compiled from Amato *et al.* (2014), Akinin *et al.* (2015) and results from this study. Shaded region in inset highlights age range of results presented in this paper.

been correlated due to conspicuous differences in metamorphic grade.

The structure and composition of the AAC terrane have been greatly influenced by an episode of Jura–Cretaceous crustal shortening, followed by extension and voluminous magmatism related to Pacific margin tectonics (e.g. Patrick 1988; Miller & Hudson 1991; Miller *et al.* 1992; Moore *et al.* 1994; Hannula *et al.* 1995; Klemperer *et al.* 2002; Akinin *et al.* 2009, 2013). In particular, Cretaceous magmatism and accompanying high-grade metamorphism have strongly overprinted the Chukotka basement rocks, which are exposed in the Velitkenay massif study area as a culmination of gneissose igneous and metamorphic rocks (Figs 2 & 3). By contrast, Cretaceous plutons are absent from Wrangel Island's exposed basement, which was metamorphosed only to greenschist facies conditions during Cretaceous deformation (Figs 2 & 3) (Miller *et al.* 2010, this volume, in press *b*).

The robustness of zircon as a geochronometer and geochemical archive (e.g. Kröner 2010) allows us to read and relate the history of basement rocks across this metamorphic gradient, despite the superimposed high-grade metamorphism and partial

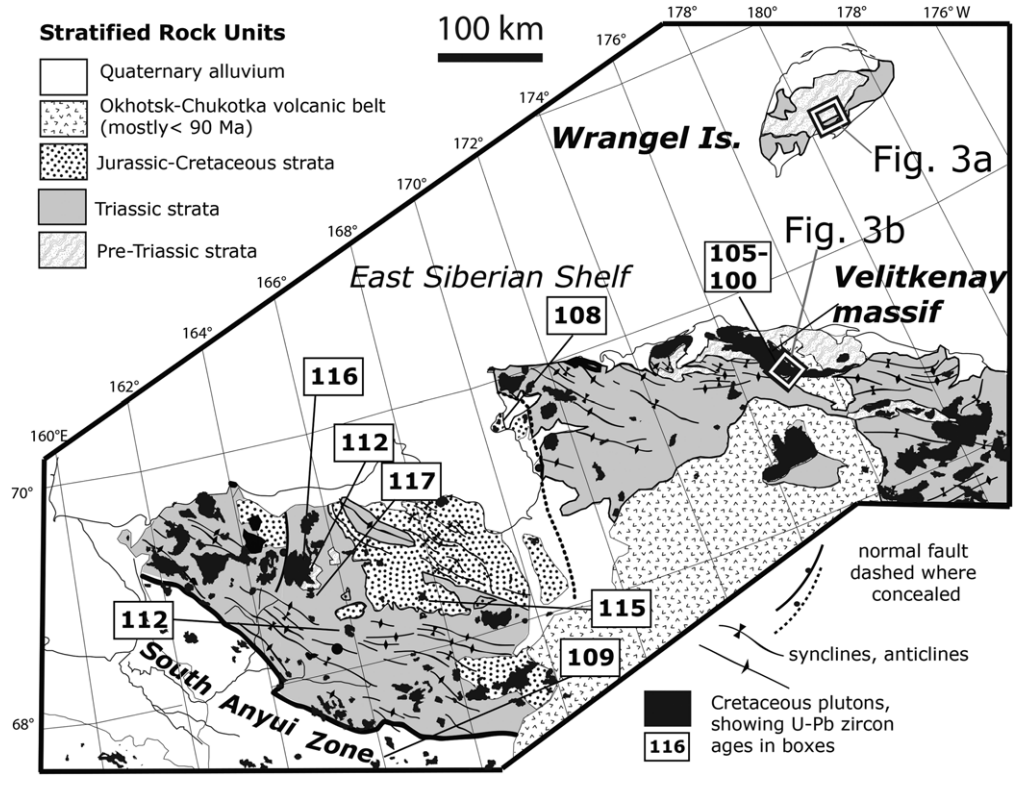

Fig. 2. Regional study area map of central Chukotka and Wrangel Island modified from Miller & Verzhbitsky (2009), highlighting the relatively limited aerial distribution of pre-Mesozoic outcrop and the pervasive distribution of Early to mid-Cretaceous plutonic and Late Cretaceous Okhotsk–Chukotka Volcanic Belt rocks across central Chukotka, which are absent from Wrangel Island. Ages of plutons in Velitkenay massif from Miller *et al.*, this volume, in press *b*

melting of rocks in Chukotka. Integrating the U–Pb geochronology of igneous rocks, O and Hf isotope geochemistry in zircon and temporal-based observations about the changing character of crustal inheritance in magmas provides insights into the history of Neoproterozoic basement rocks in the AAC terrane. These observations establish potential palaeogeographic and tectonic tie-points between the crustal section of Arctic Chukotka and other continental masses in the circum-Arctic region.

Our geochronology-based approach documents several new findings regarding the tectonic history of the Arctic. First, the correlation of the age spectrum of inherited zircons in a 703 $\pm$ 5 Ma pluton from Wrangel Island with detrital zircon signatures from other lithotectonic units in the AAC terrane suggests stratigraphic ties between distant regions of the terrane (Fig. 1). Similar detrital zircon age distributions in the pervasively deformed Nome Group metasedimentary rocks on Seward Peninsula (Fig. 1) (Till *et al.* 2014*a*, *b*) and in metasedimentary rocks of the Schist Belt of the central Brooks Range (Fig. 1) (Hoiland *et al.* this volume, in press) indicate that the AAC terrane may contain regionally correlative, pre-700 Ma stratigraphic sequences. Detrital zircon signatures from these areas have similar age peaks to Grenville–Sveconorwegian sourced Neoproterozoic strata of the Pearya terrane in the Canadian Arctic (Malone *et al.* 2014), located on the opposite side of the Amerasia Basin from the AAC terrane (Fig. 1). Analysis of zircon inheritance, combined with O and Hf isotopic compositions of 705–580 Ma (Cryogenian and Ediacaran) meta-igneous basement rocks of the AAC terrane, establishes that magmatism in the central AAC terrane exhibits temporal trends characteristic of an orogenic setting that generated increasingly primitive magma through time (i.e. an external/peripheral orogeny; Murphy & Nance 1991; Collins *et al.* 2011; Cawood *et al.* 2016). This suggests that the central AAC terrane became isolated from the input of recycled continental detritus, either as an offshore arc or an arc established on a rifted ribbon continent, during the period 705–580 Ma. In aggregate, these insights about the relationship of the AAC terrane to the other circum-Arctic terranes that comprised the northern margin

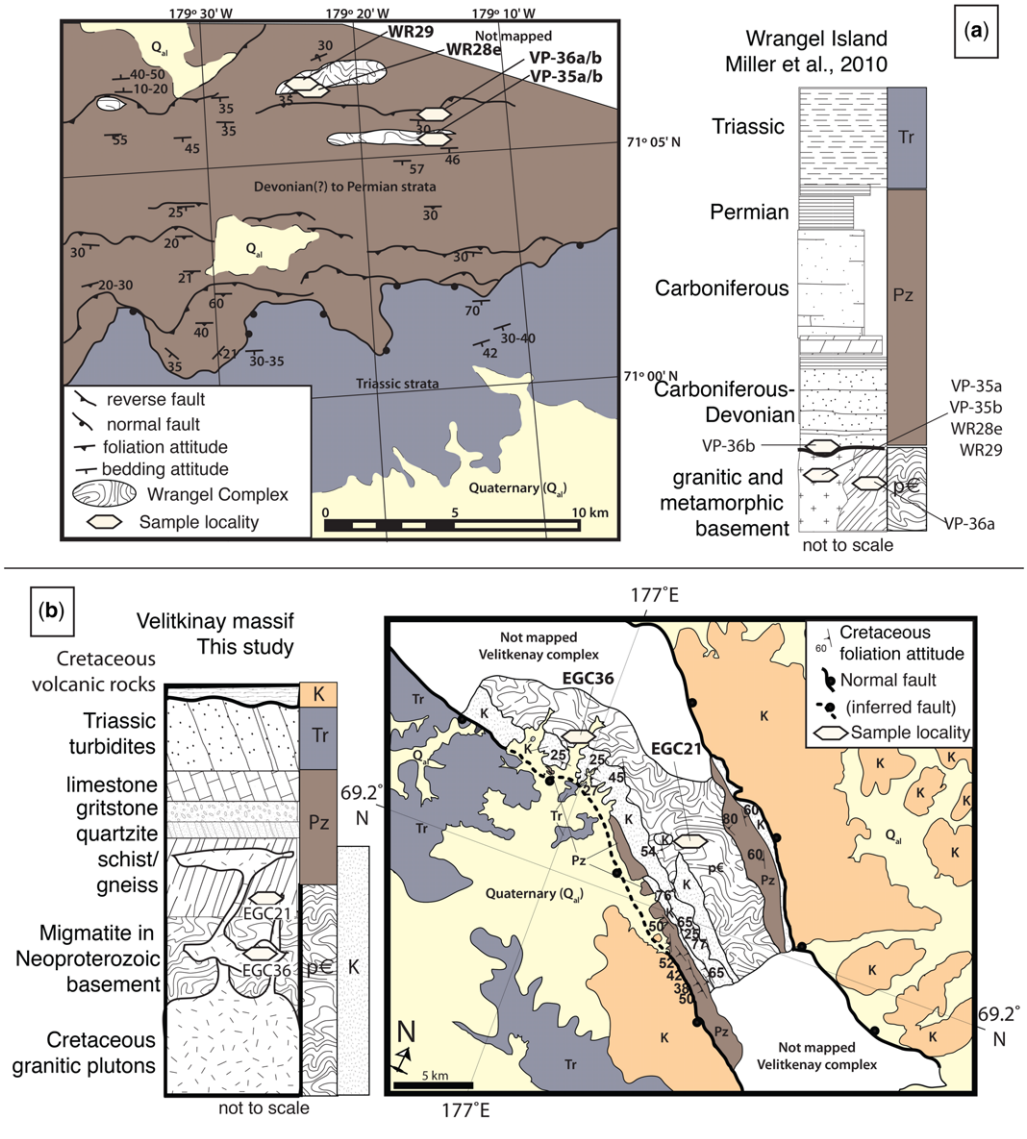

Fig. 3. Geological maps and generalized stratigraphic columns showing sample locations for each study area. (**a**) Kichshnikov River area of Wrangel Island (simplified from Miller *et al.* 2010). (**b**) Velitkenay massif in Arctic Chukotka based on previously unpublished mapping from the 2011 field season.

of Rodinia in late Neoproterozoic time are invaluable for palaeogeographic and tectonic reconstructions of the Arctic.

Geological setting

Arctic Alaska Chukotka terrane

The southern/southwestern margin of the AAC terrane in Russia is juxtaposed against the much older (3.4–2.0 Ga) Kolyma–Omolon block along the Mesozoic age South Anyui zone (Amato *et al.* 2015 and references cited therein) (Figs 1 & 2). Farther west and north, the southern boundary of the AAC terrane is projected offshore across the western part of the East Siberian continental shelf to the New Siberian Islands (Franke *et al.* 2008; Kuzmichev 2009). The DeLong archipelago has been included as part of the AAC terrane based on basement age correlations from Zhokov Island (Fig. 1) (Akinin *et al.* 2015). Voluminous volcanic deposits of the mid- to Late Cretaceous Okhotsk–Chukotka

Volcanic Belt (OCVB) obscure the South Anyui zone between Chukotka and Kolyma–Omolon east of the 168° E meridian (Fig. 2). The OCVB was generated in several distinct pulses by north-dipping subduction beneath the southern continental margin of Arctic Chukotka (Tikhomirov *et al.* 2008; Akinin & Miller 2011). Several additional episodes of crustal growth from magmatic addition and subduction accretion have occurred along the margin since Late Cretaceous time (e.g. Hourigan *et al.* 2009). This obscured southern boundary of Arctic Chukotka is proposed to cross the Bering Sea Shelf south of St Lawrence Island and to link up with the Angayucham suture zone, which delineates the southern boundary of the Alaskan part of the AAC terrane (Churkin & Trexler 1981; Nokleberg *et al.* 2000; Amato *et al.* 2015).

The oldest dated meta-igneous basement rocks in the AAC terrane are the 968 ± 5 Ma Ernie Lake orthogneiss, located in the southern Brooks Range (Fig. 1) (Amato *et al.* 2014). The next oldest are *c.* 870 Ma granitic orthogneiss and meta-volcanic rocks exposed on Seward Peninsula (Amato *et al.* 2009, 2014) (Fig. 1). These isolated exposures are succeeded, from 750 Ma and continuing to the start of the Phanerozoic, by punctuated magmatism with age gaps no greater than 30 Ma (Amato *et al.* 2014) (Fig. 1b). Although magmatism recurred in a regular and episodic manner after 750 Ma, the age interval(s) of magmatism are regionally variable (Fig. 1b). The oldest documented ages of Neoproterozoic magmatism in the non-Alaskan part of the AAC terrane are much younger than the oldest ages reported for Arctic Alaska (Fig. 1b). On Wrangel Island, Neoproterozoic magmatism is as old as 700 Ma (Cecile *et al.* 1991), which is the oldest magmatism documented in the basement of the AAC terrane outside Arctic Alaska. In the westernmost part of the AAC terrane, crustal xenoliths in Neogene lavas derived from basement rocks underlying Zhokov Island in the DeLong archipelago range from 660 to 600 Ma (Fig. 1) (Akinin *et al.* 2015). In eastern Chukotka (Koolen metamorphic complex), a broad range of ages from 670 to 565 Ma are documented (Fig. 1) (Natal'in *et al.* 1999; Amato *et al.* 2009, 2014). Farther west in mainland Chukotka, Neoproterozoic magmatism had not been reported prior to this study.

Study areas

Wrangel Island is an isolated, 7600 km^2 landmass surrounded by the vast East Siberian continental shelf of the Arctic Ocean (Fig. 1). Located 140 km north of the Arctic coastline of Chukotka, *c.* 400 km south of the shelf–slope break and nearly 1000 km east of the nearest of the New Siberian and DeLong islands (Fig. 1), Wrangel Island is a key locality for studying the composition and geological history of crust that makes up the northern flank of the AAC terrane. The Precambrian basement of Wrangel Island (the Wrangel Complex) is exposed in the core of an east–west-trending anticlinorium in the centre of the island, unconformably overlain by Palaeozoic and Mesozoic sedimentary cover (Figs 2 & 3a) (Kos'ko *et al.* 1993; Miller *et al.* this volume, in press *b*). Wrangel Complex basement rocks consist of felsic to intermediate volcanic rocks, volcaniclastic rocks, slates/phyllites, quartzites, conglomerates and very minor mafic volcanic rocks, with quartz-feldspar porphyries, gabbros, diabases, felsic dykes and sills, and granitic plutons (Kos'ko *et al.* 1993). Previous geochronological studies documented a Cryogenian age for volcanic and granitic rocks in Wrangel Complex (700 and 630 Ma; Cecile *et al.* 1991), whereas microfossils indicate middle Riphean (pre-Cryogenian) and latest Proterozoic–Early Cambrian age strata (Kos'ko *et al.* 1993 and references cited therein [in Russian]). In the study area, Devonian(?), Carboniferous, Permian and Triassic strata unconformably overlie the Wrangel Complex in a sequence that transitions from locally sourced terrigenous shallow water clastic and carbonate shelf deposits in Late Palaeozoic time to deep water siliciclastic strata in the Triassic (Fig. 3a) (Miller *et al.* 2010).

The stratigraphic section of western Chukotka is similar to Wrangel Island (e.g. Kos'ko *et al.* 1990; Ershova *et al.* 2016), but, unlike Wrangel Island, it was the site of voluminous Cretaceous magmatism and high-grade metamorphism at deeper crustal levels (Figs 2 & 3b) (Miller *et al.* 2009; Miller *et al.*, this volume, in press *b*). The Velitkenay (massif) complex (Figs 2 & 3b) is one of few areas in western Chukotka that exposes basement rocks potentially correlative to the Wrangel Complex. Here they crop out as a variably deformed metamorphic complex of schist, gneiss and migmatite of unknown protolith ages that are intruded by Cretaceous granitic rocks (Fig. 3b). Devonian, Carboniferous and Permian age strata, as well as latest Devonian to earliest Carboniferous granitic rocks, occur in scattered locations across western Chukotka (Kos'ko *et al.* 1990; Lane *et al.* 2015; Ershova *et al.* 2016) and represent the oldest dated rocks described in western Chukotka prior to this study.

Most of the area is covered by Mesozoic age rocks that consist of Triassic to Early Cretaceous deep water sedimentary rocks intruded by mid-Cretaceous plutonic rocks and/or unconformably overlain by Late Cretaceous volcanic rocks of the OCVB (Fig. 2) (Miller & Verzhbitsky 2009). Cretaceous plutons in the Velitkenay complex span *c.* 106–100 Ma (Miller *et al.*, this volume, in press *b*), coeval with widespread *c.* 118–100 Ma magmatism

in Chukotka and preceding OCVB magmatism (Fig. 2) (Miller *et al.* 2009). Biotite and hornblende $^{40}Ar/^{39}Ar$ ages from Velitkenay range from 100 to 95 Ma and exhibit well-defined step-heating plateau ages, signifying relatively fast cooling from high-grade conditions at that time (Miller *et al.* this volume, in press *b*). Deformation, metamorphism and plutonism generally intensifies with increasing stratigraphic and structural depth (Miller & Verzhbitsky 2009) and has obscured the original basement–cover relationships that are still observable on Wrangel Island (Fig. 3).

Methods

Sampled materials

Our investigation of Arctic Chukotka and Wrangel Island basement is built around analyses of nine igneous rock samples that yielded zircons with Neoproterozoic crystallization ages (Table 1). Several analytical techniques are integrated in this study: secondary ion mass spectrometry (SIMS)-based zircon U–Pb geochronology (eight samples); zircon trace element geochemistry (three samples); zircon $^{18}O/^{16}O$ isotopic analyses (three samples); and laser ablation inductively coupled plasma mass spectrometry (LA-ICP-MS) zircon Lu–Hf isotopic analyses (four samples). Collectively, these methods are used to fingerprint and correlate the age and geochemistry of Neoproterozoic magmatism and crustal inheritance that characterizes the basement of Arctic Chukotka and Wrangel Island.

Six samples were collected on Wrangel Island during 2006 and two samples were collected from the Velitkenay complex in Arctic Chukotka during 2011. An additional sample used in the study is a previously dated orthogneiss from the Koolen Lake region on the Chukotka Peninsula (sample G31) (Fig. 1), for which a zircon U–Pb crystallization age of 574 ± 9 Ma (lower concordia intercept, 2s) has been reported (Amato *et al.* 2014).

Five samples, all from Wrangel Island, are granite to granodiorite composition plutonic rocks (Table 1). Four of the five samples were collected from the Wrangel Complex basement: sample VP06-35a is a granitic xenolith enclave enclosed in a K-feldspar augen gneiss (sample VP06-35b) (Fig. 4a) and samples ELM06WR28e and ELM06WR29 are from a weakly foliated granodiorite pluton. The fifth sample (VP06-36b) is a granitic cobble from conglomerate that unconformably overlies the Wrangel Complex (Figs 3a & 4b). The sixth Wrangel Island sample (VP06-36a) is a quartz-rich meta-volcanic rock (Fig. 4c).

The basement rocks investigated from Chukotka have experienced a sufficiently high metamorphic grade during deformation that determining whether their igneous protoliths were intrusive or extrusive is problematic (Table 1). Two of the samples are from outcrops of gneissic rocks: sample G31 from Koolen Lake and a fine-grained quartzo-feldspathic, biotite-bearing rock (11EGC21) from the Velitkenay complex (Fig. 4d). The third sample (11EGC36) is an undeformed leucogranite from the migmatite zone in the Velitkenay complex, but contains xenocrystic Neoproterozoic zircons (Figs 3b & 4e).

Zircon aliquots were hand-picked from purified mineral separates produced by standard crushing, grinding, sieving, hydrodynamic, density and magnetic separation techniques on 0.25–2 kg of sample material. Zircons were mounted in epoxy, polished to expose crystal interiors, photographed under reflected light and imaged in a scanning electron microscope using a cathodoluminescence detector. For the SIMS work, the zircon mounts were gold-coated for conductivity, but the gold coating was removed by light polishing and cleaning for the LA-ICP-MS analyses.

SIMS zircon U–Pb geochronology

Prior studies of Wrangel Island basement rocks were carried out using thermal ionization mass spectrometry dating of bulk zircon separates (e.g. Cecile *et al.* 1991). SIMS zircon geochronology guided by cathodoluminescence imaging allowed pre- and syn-magmatic growth domains in zircon crystals to be distinguished and analysed (e.g. Hanchar & Miller 1993). SIMS U–Th–Pb geochronology was carried out on zircon separates from eight igneous samples (six from Wrangel Island and two from Velitkenay) to obtain an igneous crystallization age for each sample and, in selected samples with dateable inherited zircon domains, to investigate the ages of inherited material.

Zircon U–Pb ages for samples VP06-35a, VP06-35b, VP06-36a and VP06-36b were measured using the Cameca IMS 1270 large-geometry ion microprobe in the Nordsim facility at the Swedish Museum of Natural History (methodology of Whitehouse & Kamber 2005 and references cited therein). An O_2^- primary beam from the oxygen source was used, together with Kohler mode illumination of a 200 μm beam aperture to yield a *c.* 5 nA beam, evenly sputtering a 20 μm slightly ellipsoid spot on polished zircons. A 60 eV energy window was used together with 5400 mass resolution to separate $^{206}Pb^+$ from molecular interferences. A single-collector electron multiplier with an electronically gated 44 ns deadtime was used in the ion-counting mode to measure secondary ion beam intensities for masses $^{196}[Zr_2O]^+$, $^{203.5}$[background]$^+$, $^{204}Pb^+$, $^{206}Pb^+$, $^{207}Pb^+$, $^{208}Pb^+$, $^{209}[HfO_2]^+$, $^{232}Th^+$, $^{238}U^+$, $^{248}[ThO]^+$, $^{254}[UO]^+$ and $^{270}[UO_2]^+$. U/Pb ratio calibration was based on analyses of the

Table 1. *Zircon geochronology and isotope geochemistry*

Sample	Rock type	Location	Latitude	Longitude	Age (Ma)	±2s (Ma)	Age type	MSWD	$\delta^{18}O$ (‰)	±2SD (‰)	$\varepsilon Hf_{initial}$	±2SD
Plutonic												
VP06-35a	Granitic xenolith	Wrangel Island	71.0934	−179.2454	711.4	4.2	$^{206}Pb^*/238U$	1.1				
ELM06WR29[†]	Deformed granodiorite	Wrangel Island	71.1148	−179.3972	703.4	5.0	$^{206}Pb^*/^{238}U$	1.1			−3.6	1.5
ELM06WR28e	Deformed granodiorite	Wrangel Island	71.1112	−179.3877	697.3	5.0	$^{206}Pb^*/^{238}U$	1.7				
VP06-36b	Granitic clast in Palaeozoic conglomerate	Wrangel Island	71.1020	−179.2440	673.3	4.2	$^{206}Pb^*/^{238}U$	1.1				
VP06-35b	Augen gneiss	Wrangel Island	71.0934	−179.2454	619.8	6.2	$^{206}Pb^*/^{238}U$	2.5				
Volcanic												
VP06-36a	Felsic meta-volcanic rock	Wrangel Island	71.1020	−179.2440	702.0	3.7	$^{206}Pb^*/^{238}U$	1.3				
Indeterminate (igneous) protolith												
11EGC21	Biotite quartzo-feldspathic rock	Velitkenay	69.2307	177.22249	661	11	Fixed lower concordia intercept	1.3	5.87	1.32	4.2	1.3
11EGC36	Inheritance in leucogranite	Velitkenay	69.2831	176.91508	612.3	7.3	$^{206}Pb^*/^{238}U$	0.9	4.85	0.50	7.7	2.7
G31[‡]	Orthogneiss	Koolen Dome	65.9472	−171.1667	574	9	Lower concordia intercept	1.8	6.02	0.29	9.6	2.4

WGS84 datum for geographical locations.
*^{207}Pb corrected.
[†]Hf mean excludes four outlier datapoints shown in Figure 9.
[‡]Age data from Amato *et al.* (2014).

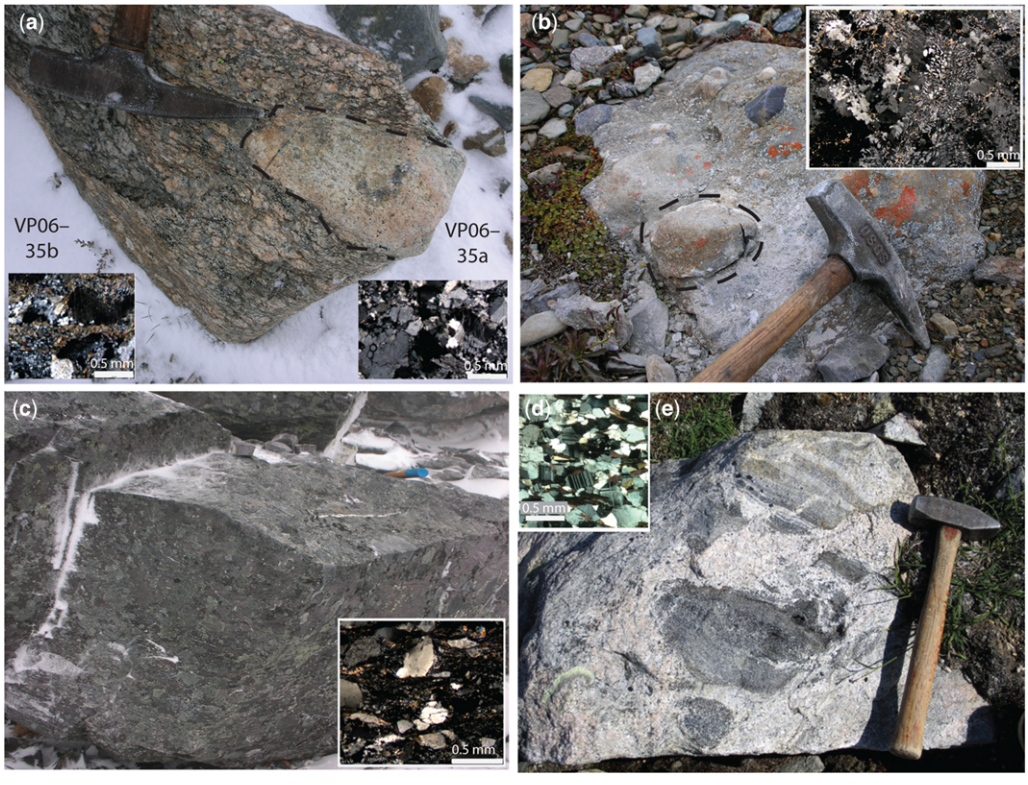

Fig. 4. Field photos and thin section images (cross-polarized light) of selected samples used in this study. (**a**) Augen gneiss sample VP06-35b with granitic enclave (outlined) VP06-35a from Wrangel Complex. (**b**) Granitic cobble VP06–36b (outlined) in Devonian(?) conglomerate that sits unconformably on the Wrangel Complex. (**c**) Meta-volcanic sample VP06-36a from the Wrangel Complex. (**d**) Thin section image from fine-grained biotite-bearing quartzo-feldspathic sample 11EGC21, exposed in gneissose part of Velitkenay complex. (**e**) Cretaceous leucogranite sample 11EGC36 with gneissose basement enclaves exposed in Velitkenay complex.

1065 Ma Geostandards zircon 91500 (Wiedenbeck *et al.* 1995). Data reduction was performed using NordAge (Whitehouse *et al.* 1999). Nordsim analyses focused on determining the crystallization age of zircons in various samples and avoided pre-magmatic inclusion domains. CL images of grains analyzed at the Nordsim facility are included as supplementary material.

Zircon U–Pb ages and selected trace element data for samples ELM06WR28e, ELM06WR29, 11EGC21 and 11EGC36 were measured by sensitive high-resolution ion microprobe-reverse geometry (SHRIMP-RG) at the Stanford USGS Micro Analysis Center at Stanford University using standard laboratory procedures for polished epoxy grain mounts. The SHRIMP-RG instrument was tuned to focus an O_2^- primary beam through a 100 μm diameter Kohler aperture, which sputtered a −5 nA, 25–30 μm diameter circular area on polished zircons. Immediately prior to data acquisition for a given spot, the primary beam was rastered for two minutes to remove gold from the intended analytical spot. During data acquisition, sputtered secondary ions were accelerated into the mass spectrometer and the relevant masses were measured on a single-collector electron multiplier in ion-counting mode. Run table acquisition parameters for the mass stations were calibrated on MAD-Green zircon, with secondary tuning parameters adjusted for best peak shape and a mass resolution of *c.* 7000 for $^{206}Pb^+$. Each analysis included four to five cycles of measurement of mass stations $^{89}Y^+$, $^{139}La^+$, $^{140}Ce^+$, $^{146}Nd^+$, $^{147}Sm^+$, $^{153}Eu^+$, $^{155}Gd^+$, $^{179}[DyO]^+$, $^{182}[ErO]^+$, $^{188}[YbO]^+$, $^{196}[Zr_2O]^+$, $^{196}[HfO]^+$, $^{204}Pb^+$, ^{204}[background]$^+$, $^{206}Pb^+$, $^{207}Pb^+$, $^{208}Pb^+$, $^{232}Th^+$, $^{238}U^+$, $^{248}[ThO]^+$, $^{254}[UO]^+$ and $^{270}[UO_2]^+$ with varying count times, resulting in each analysis requiring 12–20 minutes depending on the acquisition parameters. Calibrations of Pb/U and U/UO were performed using

the method of Ireland & Williams (2003) with R33 (419 Ma, Black *et al.* 2004) as the primary standard. Over five sessions, the 2s errors of the weighted mean of standard Pb/U calibrations were 0.6, 0.6, 0.9, 1.0 and 1.9%. Trace element concentrations were obtained from ratios of [trace element]/$^{196}[Zr_2O]^+$ normalized to MAD-Green as the concentration standard (Barth & Wooden 2010). Raw data were reduced to ratios, concentrations and ages using Squid2 (Ludwig 2009).

For results from both laboratories, concordia and weighted mean plots of reduced U–Pb data were generated with Isoplot 3.75 (Ludwig 2012) and DensityMap.R (Sircombe 2007) using uncorrected and corrected for ^{204}Pb(c) ratios of ^{207}Pb/^{206}Pb and ^{238}U/^{206}Pb for concordia diagrams and ^{207}Pb corrected ^{206}Pb/^{238}U ages for the weighted mean calculations. DensityMap.R was used to visually recognize the concordance of age clusters (Sircombe 2007). Common lead corrections were applied using a modern day average terrestrial common Pb composition, i.e.^{207}Pb/^{206}Pb = 0.83 (Stacey & Kramers 1975), where significant ^{204}Pb counts were recorded and are assumed to represent surface contamination.

SIMS oxygen isotopic ratios in zircon

^{18}O/^{16}O ratios of zircons from three samples were analysed on the Cameca 1270 IMS at the UCLA SIMS Laboratory to gain insight into their petrogenesis. The analyses were carried out in a routine fashion using the methods described by Trail *et al.* (2007), operating in the multi-collection mode with a CS^+ primary beam focused on a 15 μm sputter pit. Both the Velitkenay massif samples were analysed, in addition to the Koolen Lake orthogneiss (sample G31) (Fig. 1). For sample 11EGC36, which yielded few large zircons in the original mineral separation, the oxygen work was carried out on zircons previously dated using SHRIMP-RG that were plucked from the original U–Pb mounts, remounted, polished and imaged using standard mount preparation methods in a fresh epoxy matrix for oxygen work. For the other two samples, fresh zircons were mounted from the original mineral separates. Oxygen data were collected using R33 (Black *et al.* 2004) as a primary standard and 91500 (Wiedenbeck *et al.* 2004) as a secondary standard. Data are reported as $\delta^{18}O$ (V_{SMOW}) results, which is the ^{18}O/^{16}O ratio (±2SD) relative to Vienna Standard Mean Ocean Water measured per mil (Valley 2003). The cited precisions given for unknowns are calculated as the geometric mean of the standard reproducibility and the analytical uncertainty during analysis of the unknown. CL images of grains analyzed for oxygen isotopes are included as supplementary material.

Laser ablation Lu–Hf isotopic ratios in zircon

Laser ablation Lu–Hf zircon isotopic analyses were carried out at the Washington State University Geoanalytical Laboratory on a granodiorite sample from Wrangel Island (ELM06WR29), the two Velitkenay samples and the Koolen Lake orthogneiss sample to gain further information about their petrogenesis. Relatively large zircons that had been previously analysed during the SIMS U–Pb and/or oxygen work were targeted for Lu–Hf analysis; a few zircons from each sample that exhibited a similar cathodoluminescence appearance to the primary targets, but had no prior SIMS analyses, were included as secondary targets.

The target domains in zircons were ablated with a New Wave 213 nm Nd:YAG laser using a 40 μm diameter circular laser spot. Data acquisition and reduction protocols followed were as described in Fisher *et al.* (2014) using Mudtank zircon as the primary standard (^{176}Hf/^{177}Hf = 0.282507) and R33 (Fisher *et al.* 2014) and 91500 (Fisher *et al.* 2014) as secondary standards. $^{176}Hf/^{177}Hf_{initial}$ isotopic ratios and $\varepsilon Hf_{initial}$ results were calculated using U–Pb ages of 661, 611 and 574 Ma for the respective samples, $\lambda = 1.867 \times 10^{-11}$/yr, present day $^{176}Lu/^{177}Hf_{CHUR} = 0.0336$ and present day $^{176}Hf/^{177}Hf_{CHUR} = 0.282785$ (CHUR = chondritic uniform reservoir). A correction factor of 1.00011248 was applied to the measured ^{176}Hf/^{177}Hf ratios to obtain corrected results. Sample averages are reported as $\varepsilon Hf_{initial}$ mean values (±2SD) relative to CHUR. CL images of grains analyzed for hafnium isotopes are included as supplementary material.

Results

Neoproterozoic magmatic rocks

The U–Pb geochronology of the Wrangel Island igneous samples produced unambiguous results (Fig. 5; Table 1). Three distinctive age groups are apparent from the data. The meta-volcanic sample (VP06-36a), both granodiorite samples (ELM06 WR28e, ELM06WR29) and the granitic xenolith (VP06-35a) from the augen gneiss all yield ^{207}Pb-corrected ^{206}Pb/^{238}U weighted average ages (±2s) in the range 697.3 ± 5.0 to 711.4 ± 4.2 Ma (Fig. 5). The granitic clast (VP06-36b) from the Devonian(?) conglomerate is slightly younger (673.3 ± 4.2 Ma)(Fig. 5). The augen gneiss (VP06-35b) that contained the granitic xenolith is considerably younger, yielding an age of 619.8 ± 6.2 Ma.

In the Velitkenay massif, zircon ages from the fine-grained quartzo-feldspathic sample (11EGC21) (Fig. 4d) exhibit more discordance than any of the results from Wrangel Island and define a discordia chord (Fig. 6a). Interpretation based on additional

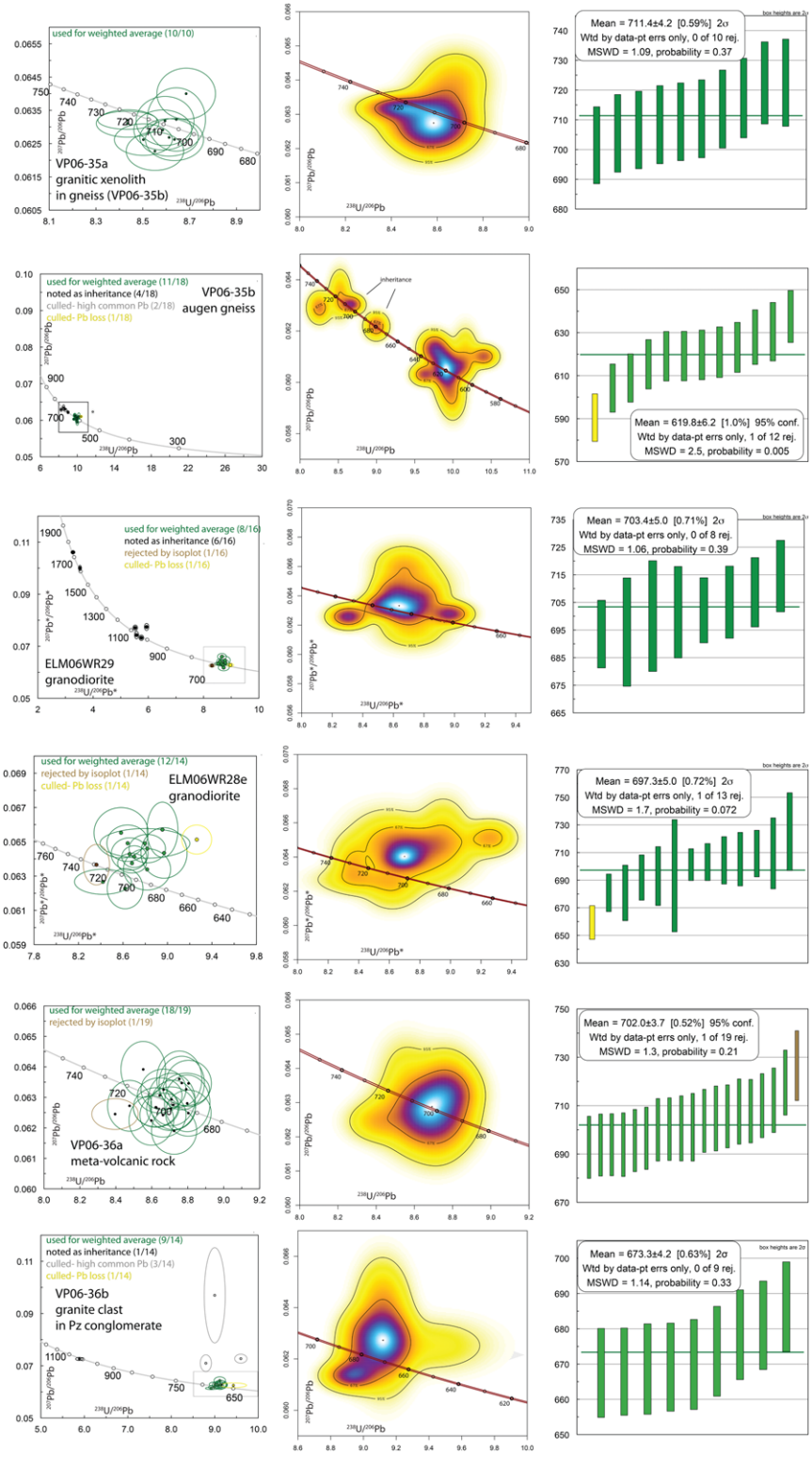
used for weighted average (10/10)
VP06-35a
granitic xenolith
in gneiss (VP06-35b)
Mean = 711.4±4.2 [0.59%] 2σ
Wtd by data-pt errs only, 0 of 10 rej.
MSWD = 1.09, probability = 0.37
used for weighted average (11/18)
noted as inheritance (4/18)
culled- high common Pb (2/18)
culled- Pb loss (1/18)
VP06-35b
augen gneiss
inheritance
Mean = 619.8±6.2 [1.0%] 95% conf.
Wtd by data-pt errs only, 1 of 12 rej.
MSWD = 2.5, probability = 0.005
used for weighted average (8/16)
noted as inheritance (6/16)
rejected by isoplot (1/16)
culled- Pb loss (1/16)
ELM06WR29
granodiorite
Mean = 703.4±5.0 [0.71%] 2σ
Wtd by data-pt errs only, 0 of 8 rej.
MSWD = 1.06, probability = 0.39
used for weighted average (12/14)
rejected by isoplot (1/14)
culled- Pb loss (1/14)
ELM06WR28e
granodiorite
Mean = 697.3±5.0 [0.72%] 2σ
Wtd by data-pt errs only, 1 of 13 rej.
MSWD = 1.7, probability = 0.072
used for weighted average (18/19)
rejected by isoplot (1/19)
VP06-36a
meta-volcanic rock
Mean = 702.0±3.7 [0.52%] 95% conf.
Wtd by data-pt errs only, 1 of 19 rej.
MSWD = 1.3, probability = 0.21
used for weighted average (9/14)
noted as inheritance (1/14)
culled- high common Pb (3/14)
culled- Pb loss (1/14)
VP06-36b
granite clast
in Pz conglomerate
Mean = 673.3±4.2 [0.63%] 2σ
Wtd by data-pt errs only, 0 of 9 rej.
MSWD = 1.14, probability = 0.33

geological evidence beyond the geochronology data is required to constrain the crystallization age and the timing of Pb loss leading to discordance. This sample exhibits a well-developed metamorphic foliation, indicating that its protolith was metamorphosed and deformed under high-grade conditions. Although metamorphism complicates protolith determination, the consistency of zircon rare earth element spectra from analysis to analysis suggests that the zircons crystallized from a common igneous source (e.g. Hoskin & Schaltegger 2003) (Fig. 6b). The O isotope ratios of the zircons also support the interpretation of a single igneous protolith. Deformation and metamorphism of the sample make the determination of a volcanic v. plutonic origin difficult, but the abundance of quartzo-feldspathic minerals indicate an intermediate to felsic composition igneous protolith (Fig. 4d).

Two approaches to determine upper and lower concordia intercept ages for the sample data (representing the ages of crystallization and Pb loss, respectively) are evaluated. The first approach involves calculating a crystallization age based only on the analytical data (independent of other geological evidence) and suggests crystallization at 681 $\pm$ 16 Ma and Pb loss at 148 $\pm$ 28 Ma (Fig. 6a). The alternative approach, fixing the lower intercept at 102 $\pm$ 4 Ma (the age range of Mesozoic magmatism independently documented in Velitkenay; Miller *et al.*, this volume, in press *b*) yields a younger (but equivalent within uncertainties) crystallization age of 661 $\pm$ 11 Ma (Fig. 6c). If the results are calculated without fixing the lower intercept, but excluding the two most discordant analyses, an intermediate result is obtained that exhibits a lower intercept age of 114 $\pm$ 57 Ma (within the error of the age of magmatism in the Velitkenay complex) and a crystallization age of 673 $\pm$ 18 Ma (Fig. 6a). In evaluating each of these results, the result calculated with the fixed lower intercept is determined to be the most robust (Fig. 6c).

The occurrence of widespread plutonism and regional metamorphism is compelling geological evidence for a Pb loss event in mid-Cretaceous time and the first (data-only, Fig. 6a) result yields a lower intercept age that is older than the independently constrained timing of magmatism by at least 15 Ma. Conversely, fixing the lower intercept to the age of the thermo-magmatic event and including all the data yields a slightly younger, more precise and still statistically sound result (Fig. 6c). It is notable that the crystallization age determined for this sample is younger than the 702 $\pm$ 12 Ma range of ages for the oldest samples in the Wrangel Complex, but overlaps the dated 673 $\pm$ 4 Ma granitic cobble from Wrangel Island.

Sample 11EGC36 from the Velitkenay massif was collected from a leucocratic phase that is widespread in the core of the metamorphic complex and commonly contains schlieren of foliated and partially melted gneiss (Fig. 4e). Although this sample was collected from an exposure of largely undeformed leucocratic granite that cuts bodies of 105 Ma foliated granite (Miller *et al.*, this volume, in press *b*), all the zircons analysed yield Neoproterozoic ages. Like sample 11EGC21, the zircons from this sample exhibit consistently similar rare earth element concentrations (Fig. 6d) and O isotope signatures, suggesting that they were derived from a common igneous source. Unlike sample 11EGC21, most of the analyses of zircons from this sample yield concordant results, with 16 of 20 analyses clustering to define a concordia age at 611.4 $\pm$ 5.7 Ma (Fig. 6e). The remaining four (more discordant) results plot near a chord with a calculated upper intercept at 609 $\pm$ 13 Ma and a fixed lower intercept at 102 $\pm$ 4 Ma (Fig. 6e). The 16 data points used in the concordia age calculation yield a ^{207}Pb-corrected $^{206}Pb/^{238}U$ weighted mean age of 612.3 $\pm$ 7.3 Ma with an asymmetrical skew towards younger ages in the population, probably reflecting some Pb loss (Fig. 6f). It is notable that the age of this zircon population is within the error of the age determined for the augen gneiss from Wrangel Island (VP06-35b) (Fig. 5). Unlike that sample, which also contained inheritance of >660 Ma zircons, none of the zircons from 11EGC36 yielded ages older than this youngest age group.

Detrital zircon inheritance

Most zircons in granodiorite sample ELM06WR29 contain inherited domains clearly recognizable in cathodoluminescence images (Fig. 7). After

Fig. 5. SIMS geochronology plots of crystallization ages for samples from Wrangel Island. First column shows Tera-Waserberg style concordia results, plotted using Isoplot 3.75 (Ludwig 2012) with error ellipses shown at 68.3% (1s) confidence. Second column shows density distribution mapping of data (Sircombe 2007) from each sample shown in the first column, illustrating the concordance of inheritance (e.g. sample VP06–35b). Contour intervals on density distributions at 67 and 95% confidence levels. Inset boxes for samples VP06-35b, VP06-36b and ELM06WR29 in first column show area of density distribution plot. Third column shows ^{207}Pb-corrected $^{206}Pb/^{238}U$ weighted average ages calculated using Isoplot 3.75 (Ludwig 2012) with individual data point error bars shown at 2s. Results shown for sample ELM06WR29 are from analysis of zircons on mount ELM4 (whereas data shown in Fig. 7 are from mounts ELM4 and ESG24). Asterisk designates ^{204}Pb-based correction applied to isotopic ratios. MSWD, mean square of weighted deviates.

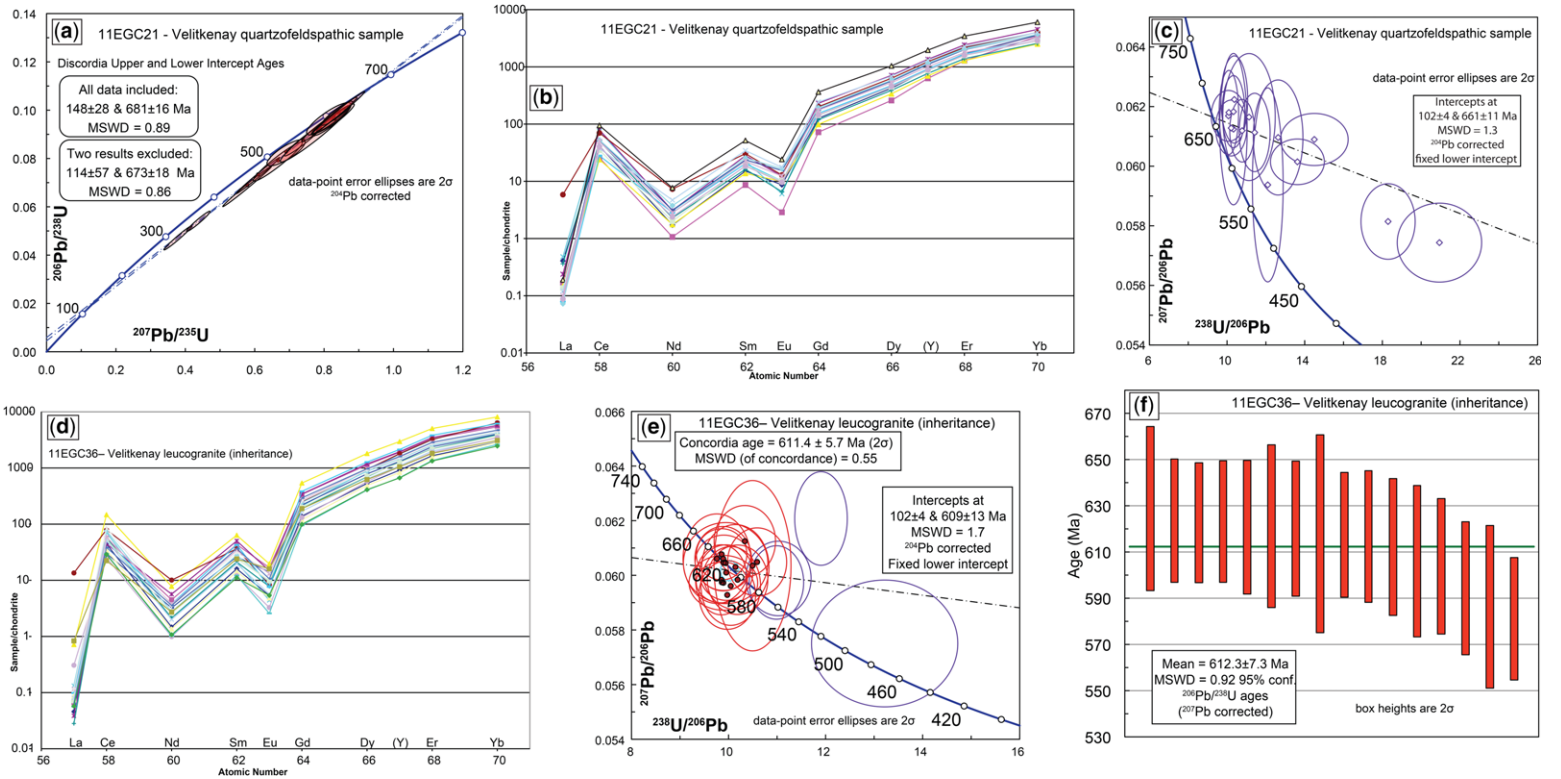

Fig. 6. SIMS zircon geochronology and trace element geochemistry results from Velitkenay massif samples, central Chukotka. (a–c) Biotite-bearing quartzo-feldspathic sample 11EGC21. (**a**) Conventional concordia plot of ^{204}Pb-corrected results, created with Isoplot 3.75 (Ludwig 2012). (**b**) Chondrite-normalized rare earth element concentrations of individual zircon analyses showing an overall consistent and typical igneous pattern (e.g. Hoskin & Schaltegger 2003). (**c**) Tera-Waserberg plot of data using fixed lower intercept based on the timing of peak metamorphism in the Velitkenay massif. (d–f) Undeformed leucogranite sample 11EGC36 with Neoproterozoic age inherited zircons. (**d**) Chondrite-normalized rare earth element concentrations of individual zircon analyses showing a similar pattern to sample 11EGC21, also suggesting that these zircons were derived from an igneous protolith. (**e**) Tera-Waserberg concordia plot of uncorrected for common Pb results created with Isoplot 3.75 (Ludwig 2012) showing calculated concordia and upper intercept results of inheritance in this sample. (**f**) ^{207}Pb-corrected ^{206}Pb/^{238}U ages showing weighted average result for inheritance that exhibits some indication of Pb loss in the younger part of the population. MSWD, mean square of weighted deviates.

determining the crystallization age of this sample by analysing the rim domains, additional zircons were mounted for the analysis of core ages. The geochronology results span a range of predominantly Mesoproterozoic ages and nearly concordant isotope ratios (Fig. 7). About 50% of the inherited zircons from ELM06WR29 are <1.3 Ga and 90% are <1.8 Ga (Fig. 7). Although several analyses yielded slightly discordant ($>-5\%$ to $<+10\%$) Pb/U and Pb/Pb ages <1 Ga, the uncertainties (2s) of these results all range as old as 1 Ga. As shown in the histogram and probability density plot inset (Fig. 7b), the overall spectra are remarkably similar whether the dataset only includes the most concordant analyses or also includes some discordant analyses.

Evaluating inheritance results from sample ELM06WR29 requires making some assumptions about the physical mechanism by which the pre-magmatic (i.e. inherited) zircons were incorporated and preserved in the granodiorite host rock. The numerous age peaks observed between 1.0 and 1.8 Ga suggest that this intrusion incorporated crustal sources that contained a well-mixed population of zircons, such as expected from siliciclastic sedimentary rocks. The relative lack of discordance indicates that the pre-magmatic zircons did not experience protracted high-grade conditions of metamorphism expected at the depth in the crust where the granodiorite magma was generated. Thus we suggest that the inherited zircons were incorporated at supracrustal depths and the spectrum of inherited, predominantly concordant, ages is a proxy for the detrital zircon signature of the strata the pluton intruded.

The youngest inherited ages from ELM06WR29 were used to constrain the depositional age of the youngest strata intruded by the pluton. Because the youngest U–Pb ages exhibit variable degrees of discordance, both $^{206}Pb/^{238}U$ and $^{207}Pb/^{206}Pb$ ages were examined in this process. The three youngest, reliably concordant ($<+5\%$ and $>-5\%$

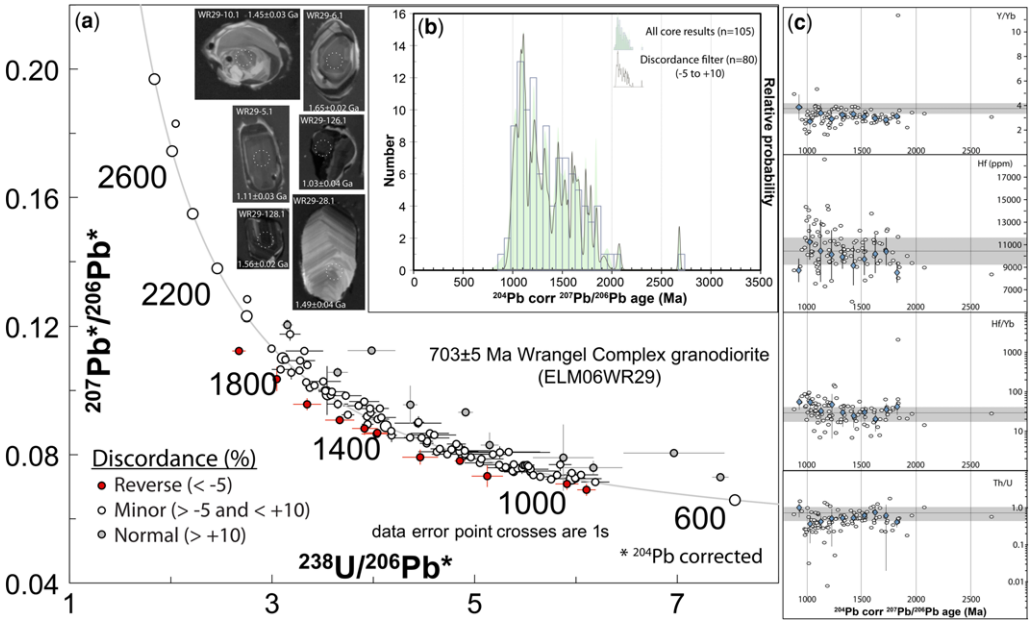

Fig. 7. SIMS (SHRIMP-RG) inheritance results from granodiorite sample ELM06WR29 from Wrangel Island. (**a**) ^{204}Pb-corrected Tera-Waserberg concordia plot of inheritance data plotted with Isoplot 3.75 (Ludwig 2012), symbolized according to discordance. Error crosses are 1s. Cathodoluminescence images of selected inherited zircon domains from this sample that yielded concordant results. Dotted circle shows sputter pit location (25 μm diameter). Age uncertainty shown at 2s. (**b**) Relative probability and histogram plot of ^{204}Pb-corrected $^{207}Pb/^{206}Pb$ ages of inherited domains in zircons created with Isoplot 3.75 (Ludwig 2012). Filled relative probability curve and histogram show all data and outline shows relative probability curve for concordance-filtered data;. (**c**) Plots of trace element data from inherited domains ($n = 105$) v. ^{204}Pb-corrected $^{207}Pb/^{206}Pb$ age results. Ellipses plot trace element concentration or ratio v. best estimate of measured age (e.g. 1223 ± 19 Ma plotted at 1223 Ma). Diamond symbols and error bars plot arithmetic mean and standard deviation of ellipse data in 100 myr age bins starting at 925 ± 50 Ma (see text). Horizontal line and grey shaded region plot arithmetic mean and standard deviation of syn-magmatic results from the sample, respectively.

discordance) $^{206}Pb/^{238}U$ results (965 ± 42, 984 ± 54 and 994 ± 82 Ma) yield a weighted mean age of 975 ± 31 Ma (mean square of weighted deviates (MSWD) = 0.3). This result excludes three ages that are >+5% discordant (963 ± 86 Ma, +12% discordant; 808 ± 16 Ma, 21% discordant; 852 ± 108 Ma, 30% discordant) and one age <−5% discordant (981 ± 28, −10% discordant). Of these four, it is notable that the two ages with lower discordance do overlap in uncertainty with the weighted mean result. The three youngest $^{207}Pb/^{206}Pb$ results (899 ± 102, 969 ± 48 and 994 ± 46 Ma) yielded a nearly identical weighted mean age of 975 ± 32 Ma (MSWD = 1.3). These results, coupled with the age obtained for pluton crystallization, indicate that the youngest supracrustal strata intruded by the pluton were deposited between 975 ± 32 and 703 ± 5 Ma.

The selected trace element geochemical concentrations and ratios (Hf, Th/U, Y/Yb and Hf/Yb) of inherited zircons in ELM06WR29 are shown in Figure 7c. As a simple test of the central tendency and variability of these results through time, we calculated an arithmetic mean and standard deviation of the data at ten discrete 100 myr intervals, beginning with the interval 975–875 Ma (Fig. 7c). Several age measurements overlap multiple age bins due to analytical uncertainty, so each data point is included in a single bin determined by the best estimate of the age value (e.g. spot WR29(C)-20.1 yielded an age of 1474.9 ± 33.9 Ma and is included in the bin 1375–1475). Because ≤2 grains fall in any bin older than 1775–1875 Ma, those intervals and their data are excluded from the calculations (Fig. 7c). The arithmetic mean and standard deviation of syn-magmatic results from the granodiorite ($n = 33$) are shown for comparison in the background (Fig. 7c). The binned results exhibit increasing mean Hf and Hf/Yb and decreasing mean Th/U ratios from 1.5 to 1.0 Ga (Fig. 7c). A reversal in the trends of mean Hf, Y/Yb and Th/U is observed in the youngest (975–875 Ma) bin ($n = 3$). Relative to the syn-magmatic results, the inheritance results exhibit lower average Y/Yb and Th/U ratios, but less pronounced deviation in Hf and Hf/Yb ratios (Fig. 7c).

Oxygen isotopes

A total of 42 of 45 R33 standard analyses yielded an uncorrected average $\delta^{18}O$ value of +6.05 ± 0.36‰ (all uncertainties reported as two standard deviations). Three R33 analyses were discarded because they yielded $\delta^{18}O$ values around +8‰. All results were divided by a correction factor of *c.* 1.09 so that the average $\delta^{18}O$ value of R33 analyses equalled the published value of +5.55‰ (Black *et al.* 2004). This resulted in a marginally low average value (but still within the two standard deviation error envelope) for the experimental value of zircon standard 91500 relative to the published value (+9.75 ± 0.34‰ v. 10.07‰; Wiedenbeck *et al.* 2004). For 91500 and the unknowns, the uncertainty reported is twice the standard deviation of the population of individual results. The population means for unknowns are reported in Table 1.

The 661 ± 11 Ma sample from the Velitkenay complex (sample 11EGC21) yielded results ranging from +4.49 ± 0.10‰ to +6.19 ± 0.11‰ (mean +5.87 ± 1.32‰, $n = 11$) (Fig. 8). If the three lightest results are excluded, the uncertainty decreases by a factor of >2.5, yielding a result of +5.95 ± 0.48‰. The 612 ± 7 Ma inherited zircon population in the undeformed leucocratic granite (11EGC36) yielded a slightly lighter and less scattered set of results ranging from +4.28 ± 0.12‰ to +5.18 ± 0.10‰ (mean +4.85 ± 0.50‰, $n = 12$) (Fig. 8). Excluding the lightest result yields a slightly more precise result of +4.90 ± 0.32‰. For the 574 ± 9 Ma Koolen Lake orthogneiss (sample G31 from Amato *et al.* 2014), the results range from +5.73 ± 0.08‰ to +6.24 ± 0.14‰ (mean +6.02 ± 0.29‰, $n = 16$), which overlaps the result from the Velitkenay orthogneiss, but is heavier in ^{18}O (beyond the uncertainty limits) than the 612 ± 7 Ma zircon population (Fig. 8). Likewise, the results from the older two zircon populations are within the +5.3 ± 0.3‰ range documented for zircon in equilibrium with the mantle (Valley 2003), whereas the Koolen Lake population is slightly heavier (Fig. 8). However, given that the Koolen orthogneiss contains inherited zircons that yield $^{207}Pb/^{206}Pb$ ages as old as 1.7 Ga (Amato *et al.* 2014), it stands to reason that some crustal component is contributing to the magma geochemistry of this sample. Although both core and rim domains were analysed in three zircons from sample G31, the variation between zircon growth zones is <0.5‰, although in each of the three grains the rims exhibited heavier results than the cores.

Hafnium isotopes

The following results were obtained for the secondary standards (the mean ± 2 standard deviation results of the solution multi-collector ICP-MS analyses of Fisher *et al.* (2014) are shown in parentheses): R33, +7.1 ± 0.9 (+8.0 ± 0.7); and 91500, +6.3 ± 1.3 (+6.9 ± 0.4). The population means for the unknowns are reported in Table 1.

The granodiorite sample from Wrangel Island (sample ELM06WR29) was the most problematic sample to analyse because four of the eight zircon grains analysed were drilled through by the laser and yielded <30 s of data for each analysis. The results of the remaining four analyses ranged from

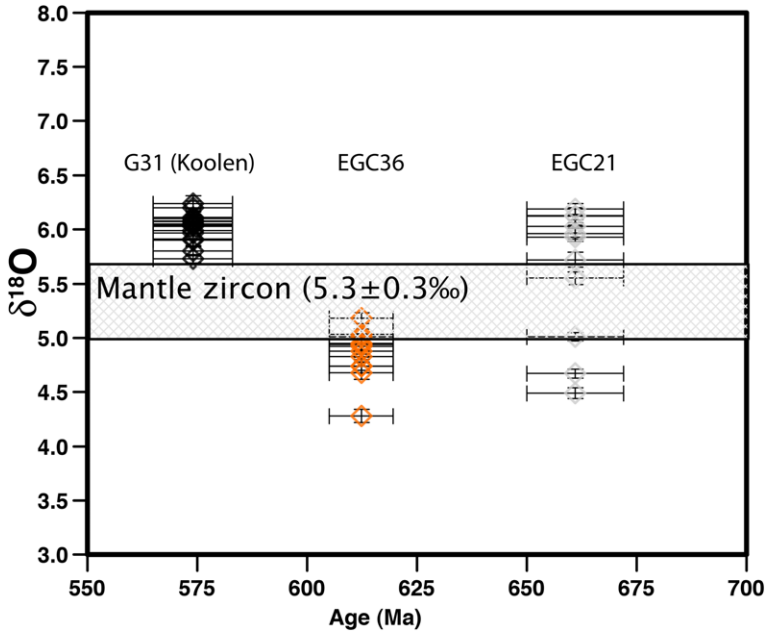

Fig. 8. Oxygen isotope results plotted as $\delta^{18}O$ v. protolith crystallization age from Velitkenay samples and Koolen orthogneiss sample G31 (Amato *et al.* 2014). Mantle zircon range ($\pm 2\ \sigma$) from Valley (2003) shown for comparison.

-4.7 ± 1.1 to -2.9 ± 1.2 (mean -3.6 ± 1.5), which are the least radiogenic (i.e. most negative in $\varepsilon Hf_{initial}$) results observed in the study (Fig. 9). For sample 11EGC21, the results ranged from $+3.0 \pm 1.3$ to $+5.3 \pm 1.1$ (mean $+4.2 \pm 1.3$, $n = 10$) (Fig. 9). The inherited zircons in sample 11EGC36 yielded a slightly more radiogenic and scattered set of results ranging from $+6.7 \pm 1.4$ to $+10.2 \pm 1.1$ (mean $+7.7 \pm 2.7$, $n = 8$) (Fig. 9). For the Koolen Lake orthogneiss (sample G31 from Amato *et al.* 2014), the results ranged from $+7.6 \pm 1.4$ to $+11.5 \pm 1.0$ (mean $+9.6 \pm 2.4$, $n = 10$) (Fig. 9). Thus the least and most radiogenic ratios are found in the oldest and youngest zircon populations, respectively (Fig. 9). In aggregate, these data demonstrate that the Hf isotopic composition of these central AAC terrane magmas increasingly trend towards depleted mantle-like signatures (Vervoort & Bilchert-Toft 1999) over 125 Myr in Neoproterozoic time (Fig. 9).

Discussion

Crustal inheritance patterns in magmatic rocks of the AAC terrane

Crustal inheritance in granitic magmas, and how this inheritance changes through time, can be determined by zircon geochronology and isotope geochemistry. The results from this study indicate several distinct types of inheritance. The inheritance that occurred early in the time span of magmatism (e.g. the 703 ± 5 Ma granodiorite sampled from the Wrangel Complex; sample ELM06WR29) is likely to be detrital zircons from supracrustal strata that contaminated the magma during emplacement. The recycling of igneous (rather than metasedimentary) basement 80 myr later, in 620 ± 6 Ma K-feldspar bearing augen gneiss from the Wrangel Complex (sample VP06-35b), is indicated by the inheritance of a 711 ± 4 Ma granitic xenolith (VP06-35a) (Fig. 4a) and xenocrystic zircons that yield mostly concordant ages between 710 and 680 Ma (Fig. 5).

In far eastern Chukotka, Amato *et al.* (2014) documented two Neoproterozoic episodes of crustal recycling: leucosome generation during partial melting of the Neoproterozoic Koolen Lake paragneiss basement at 666 ± 5 Ma (zircon U–Pb) and rare *c.* 1.7 Ga zircons in the 574 ± 9 Ma Koolen Lake orthogneiss. Zircons in the undeformed leucogranite sample 11EGC36, which yielded a 612 ± 7 Ma crystallization age, are evidence of a much younger episode of basement recycling during the mid-Cretaceous peak metamorphism and migmatite generation in the Velitkenay massif. Gneiss enclaves in Cretaceous leucogranite are further

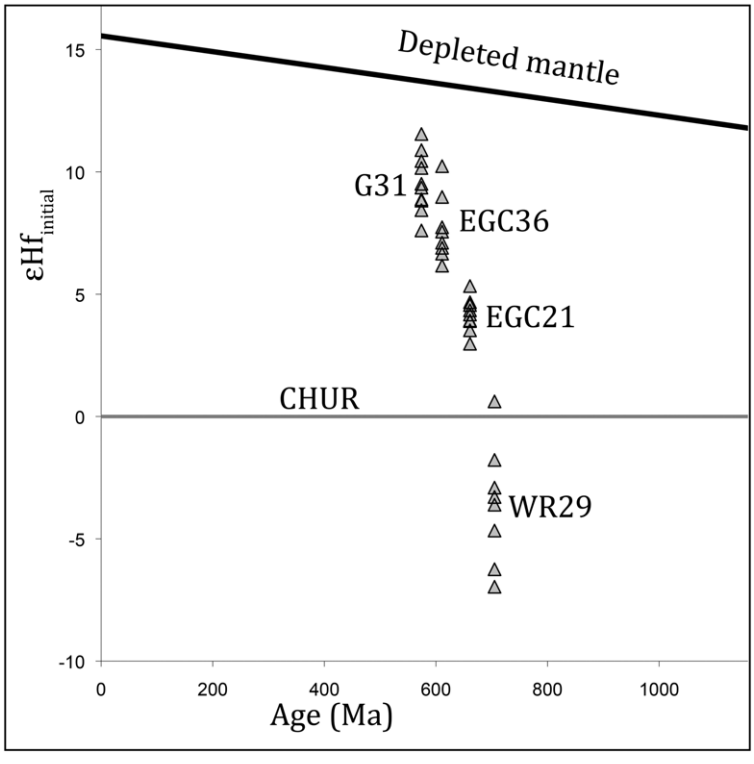

Fig. 9. Hf isotope results plotted as $\varepsilon Hf_{initial}$ v. protolith age for Wrangel Complex sample ELM06WR29, both Velitkenay samples and Koolen orthogneiss sample G31. Depleted mantle $\varepsilon Hf_{initial}$ trajectory calculated using isotope ratios reported in Vervoort & Patchett (1996). CHUR, chondritic uniform reservoir.

evidence of the incomplete assimilation of basement (Fig. 4e).

Taken together, these observations provide evidence for multiple, and temporally discrete, episodes of reworking of crustal and crustal-derived material in the Arctic Chukotka basement during Neoproterozoic magmatism, followed by an episode of remobilization of these older rocks during a mid-Cretaceous tectono-thermal event 0.5 Gyr later.

Correlation of Wrangel inheritance data across the AAC terrane

The age spectrum of inherited zircons in sample ELM06WR29 (Fig. 7) is most simply interpreted as a detrital zircon age spectrum of assimilated sedimentary rocks. This allows palaeogeographical correlations of the Wrangel Complex metasedimentary basement to other parts of the AAC terrane based on detrital zircon age spectra (Fig. 10). Pervasively deformed metamorphic rocks of the Nome Complex on the Seward Peninsula (Till *et al.* 2014*a*, *b*) and central Brooks Range Schist Belt strata (Hoiland *et al.* this volume, in press) are similar in the sense that they also contain predominantly 0.9–2.1 Ga detrital zircon with a Late Mesoproterozoic age peak (Fig. 10).

On Seward Peninsula (Fig. 1), this predominantly Mesoproterozoic age spectrum (classified as the 'Mesoproterozoic theme'; Till *et al.* 2014*a*, *b*) has been reported in four samples from two different map units that are interpreted as Palaeozoic age (as young as Devonian), despite the absence of Palaeozoic age zircons in any of the samples (Till *et al.* 2014*b*). Age assignments are based on fossil data from the surrounding rocks and stratigraphic interpretations about the deformed sequences (Till *et al.* 2014*b*).

Three of those four samples are assigned to the calcareous metasiliceous unit (Fig. 10) and are interleaved with other metasedimentary rocks that contain Middle Devonian age zircons (Till *et al.* 2014*a*, *b*). Till *et al.* (2014*a*, *b*) report that calcareous metasiliceous 'Mesoproterozoic theme' samples (Fig. 10) were deposited in a restricted subbasin associated with the formation of the Aurora Creek zinc deposit. An Early Devonian maximum age is inferred from the youngest detrital zircons

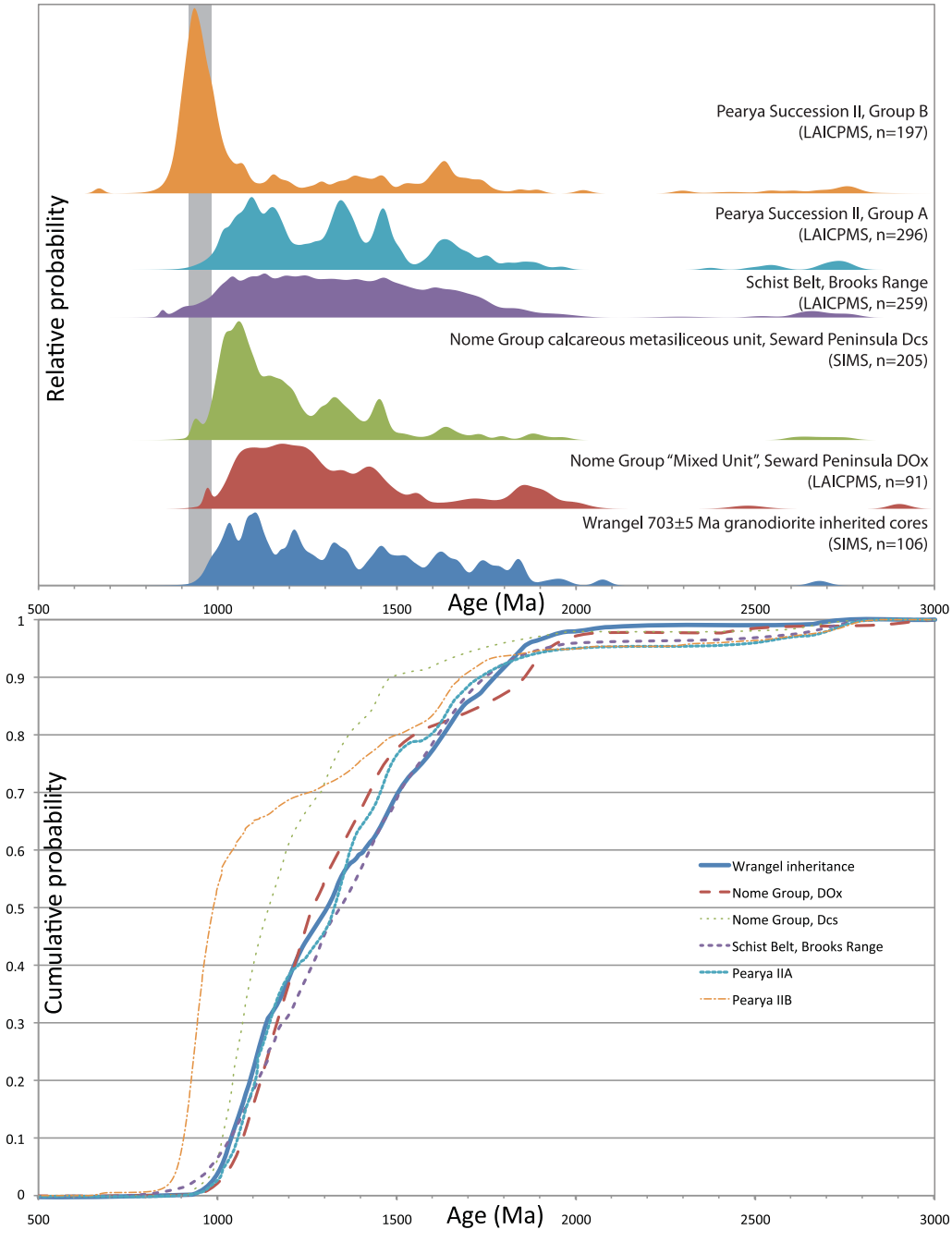

Fig. 10. Normalized probability plot (Gehrels 2010*a*; top) and cumulative probability plot (Gehrels 2010*b*; bottom) of inheritance ages in Wrangel Complex sample ELM06WR29 compared with correlative AAC strata and similar age strata from the Pearya terrane. Grey shaded region in normalized probability plot is 980–920 Ma. Sources of detrital zircon data: Nome Group, Till *et al.* (2014*b*); Pearya, Malone *et al.* (2014); Brooks Range Schist Belt, samples 13-CH-BR03b and 13-CH-BR04/A from Hoiland *et al.* (this volume, in press).

in strata that host the deposit (Till *et al.* 2014*b*), although none of the calcareous metasiliceous 'Mesoproterozoic theme' samples have Palaeozoic zircons (Fig. 10). In the model of Till *et al.* (2014*b*), 'Mesoproterozoic theme' calcareous metasiliceous strata were locally derived from associated fault scarps that recycled basement strata into the sub-basin during Palaeozoic time, yet contain no Palaeozoic zircon.

Strata with the 'Mesoproterozoic theme' are also observed in another Nome Group unit (the 'mixed unit'), which exhibits a broad range of protolith ages with uncertain stratigraphic relationships to one another (Till *et al.* 2014*a*, *b*). That 'Mesoproterozoic theme' sample comes from a white metaquartzite layer in a marble-rich, structurally lower part of the 'mixed unit' that consists of Ordovician through Devonian or younger strata (Till *et al.* 2014*a*, *b*).

In the central Brooks Range, two Schist Belt samples collected along the John River (near Ernie Lake; Fig. 1) also yield predominantly 'Mesoproterozoic theme' spectra (Fig. 10) and are structurally interlayered with dated or inferred Devonian age rocks (Hoiland *et al.* this volume, in press). Like the Nome Group strata on Seward Peninsula, constraining the depositional age of these Schist Belt strata based on stratigraphic relationships is complicated by deformation (Hoiland *et al.* this volume, in press). Hoiland *et al.* (this volume, in press) interpret them as more likely to be of Neoproterozoic age than Devonian, or at least as having been recycled from local Neoproterozoic basement.

The similar age spectrum of inherited zircon in 703 ± 5 Ma granodiorite from Wrangel Island (Fig. 10) and the absence of detrital zircon ages <700 Ma in Nome Group and Schist Belt 'Mesoproterozoic theme' strata (Fig. 10) suggest that either the interpretation of Palaeozoic depositional ages is incorrect or that these strata are recycled from Neoproterozoic strata in the local basement. The first case is plausible if these 'Mesoproterozoic theme-bearing' samples are Neoproterozoic, not Devonian, but are structurally juxtaposed with Palaeozoic rocks containing Devonian detrital zircon signatures. In the western Brooks Range (Fig. 1), structural geometries supporting this interpretation have been documented in at least two localities. The out-of-sequence structural juxtaposition of Proterozoic and Palaeozoic strata is exposed in the western Brooks Range at Mt Angayukaqsraq (Fig. 1) (Till *et al.* 1988). Nearby, 705 ± 35 Ma granite and its Proterozoic country rock comprise the structurally lowest component of the (Brookian) Schist Belt in the Kallarichuk Hills (Fig. 1), interpreted as stratigraphic basement exposed in structural windows, lateral ramps and as out-of-sequence thrusts (Karl & Aleinikoff 1990). Till *et al.* (2014*b*) also describe Neoproterozoic and suspected Neoproterozoic metasedimentary rocks in the southwestern Brooks Range that '... yielded detrital zircon much like the Mesoproterozoic theme' (Till & Dumoulin, unpublished data).

In the alternative case, if the Seward Peninsula (and/or Schist Belt) units are indeed Palaeozoic in age, as suggested by Till *et al.* (2014*a*, *b*), then their detrital zircon signatures indicate that they were recycled from strata that correlate with the Wrangel inheritance. In either case, the documentation of these correlative age spectra in several locations across the AAC terrane represents the first evidence of a possibly regionally extensive suite of metasedimentary strata within the Neoproterozoic basement rocks of the AAC terrane (Fig. 10).

Circum-Arctic correlation of Neoproterozoic strata in the AAC terrane

The correlation of AAC terrane basement rock units to those elsewhere in the circum-Arctic region is complicated by the inaccessibility and broad size of the continental shelves rimming the Arctic (e.g. the Barents Shelf, Marello *et al.* 2013; the Chukchi Shelf, Klemperer *et al.* 2002; the Northwind Ridge, Grantz *et al.* 1998; the Chukchi Borderland, Brumley *et al.* 2014). Despite this, several new insights are now possible given the Wrangel inheritance data and similar detrital zircon signatures reported from Schist Belt and Nome Group rocks containing the 'Mesoproterozoic theme' of Till *et al.* (2014*a*, *b*). Across the circum-Arctic region, Neoproterozoic strata with detrital zircon ages similar to the Wrangel inheritance and the 'Mesoproterozoic theme' are common, but, in contrast with these AAC terrane strata, many of those strata exhibit age peaks older than 1.6 Ga (e.g. fig. 10 in Malone *et al.* 2014; fig. 3 in Zhang *et al.* 2015). Provenance comparisons between the AAC and Pearya terranes (Malone *et al.* 2014) establish key similarities and contrasts in Neoproterozoic stratigraphy on opposite flanks of the Amerasia Basin (Figs 1 & 10).

The depositional age range proposed for this Neoproterozoic AAC terrane sequence is broadly coeval to a *c.* 1030–710 Ma period of sedimentation and orogeny (Valhalla orogen) that has been documented in numerous Arctic and North Atlantic Caledonide terranes (e.g. Cawood *et al.* 2010). The AAC terrane age spectra are remarkably similar to strata from the Pearya terrane (Malone *et al.* 2014) (Fig. 10), which have been correlated as part of the Valhalla orogen (Cawood *et al.* 2016). The Grenville–Sveconorwegian orogenic belts that formed on the margins of Baltica and Laurentia during the assembly of Rodinia have been suggested as provenance of those Pearya strata and similar detrital zircon signatures in the Valhalla orogen (Fig. 11) (Kirkland *et al.* 2007; Malone *et al.* 2014).

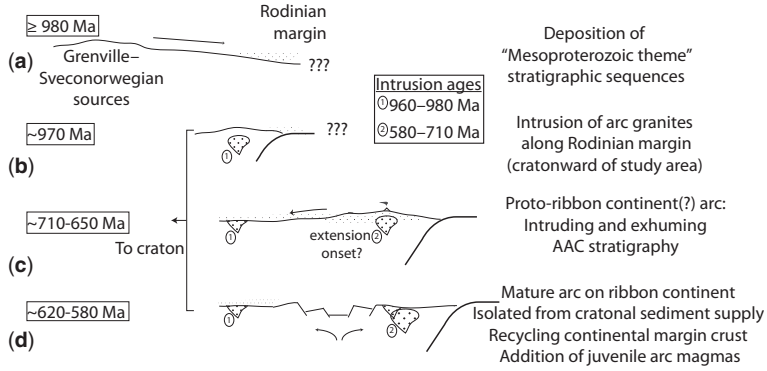

Fig. 11. Hypothetical tectonic evolution of the AAC terrane during Neoproterozoic time based on data from this study and references in text. Arrows above surface show direction of inferred sediment transport. (**a**) Delivery of sediments with Grenville–Sveconorwegian sources to Rodinian margin. (**b**) Development of 980–920 Ma arc magmatism along Rodinian margin, inboard of Arctic Chukotka/Wrangel Island crust. (**c**) Establishment of Cryogenian arc on Arctic Chukotka/Wrangel Island crust, outboard of 980–920 Ma arcs. (**d**) Arc built on rifted fragment of Rodinian margin isolated from craton-sourced sediments by a back-arc basin.

Trace element data from inherited detrital zircons in the 703 ± 5 Ma granodiorite sample provide independent evidence that AAC terrane strata have some orogenic belt provenance. Increasing Hf and Hf/Yb ratios, coupled with the decreasing Th/U ratios observed from 1.3 to 1.0 Ga (Fig. 7c), indicate progressively younger zircons in the inherited population formed from more evolved/fractionated magmas relative to the older magmas (e.g. Barth & Wooden 2010; Claiborne *et al.* 2010). The detrital zircon geochemical trends record a prolonged interval characterized by an increase in crustal recycling signatures (Fig. 7c), consistent with the Late Mesoproterozoic assembly of Rodinia (e.g. Spencer *et al.* 2015), further strengthening ties between the AAC terrane and these sources (Fig. 11).

The 975 ± 32 Ma youngest zircon age population in our data overlaps the timing of magmatism that has been dated in the Brooks Range (Amato *et al.* 2014), Pearya terrane (Malone 2012; Malone *et al.* 2014), the Northwest terrane of Svalbard (Pettersson *et al.* 2009), the Farewell terrane of central Alaska (Bradley *et al.* 2014), the Kalak Nappe Complex in Finnmark (Kirkland *et al.* 2006) and Central Taimyr (Vernikovsky *et al.* 2011) (Fig. 1). Malone *et al.* (2014), building on the work of Cawood *et al.* (2010) and Kirkland *et al.* (2011), suggested a palaeogeographical model in which arc magmatism occurred along parts of the Rodinian margin of Siberia, Laurentia and Baltica in the time span 980–920 Ma (Fig. 11). The few 0.9–1.0 Ga zircon ages in AAC terrane strata suggest a linkage to these magmatic sources (whether by primary proximity or sediment recycling), further strengthening an association with the Valhalla orogen. However, the stratigraphic interval in the Pearya terrane that bears remarkably similar spectra (Succession IIA of Malone *et al.* 2014) also contains strata dominated by a *c.* 970 Ma age peak (Fig. 10) (Succession IIB of Malone *et al.* 2014), as do numerous other Valhalla orogen strata (Cawood *et al.* 2007; Bingen *et al.* 2011). At present, no strata that also exhibit a primary age peak at 970 Ma have been documented in the AAC terrane. This is a distinct difference between detrital zircon signatures from AAC terrane strata and from strata in these other locales.

Neoproterozoic magmatism in the central AAC terrane: a ribbon continent setting?

The integrated U–Pb, O and Hf isotopic data from 710 to 580 Ma igneous zircons studied across the AAC terrane suggest that the magmas generated during late Neoproterozoic time reflect consistent, volumetrically important additions of isotopically juvenile (i.e. mantle-derived) material to a more evolved crustal infrastructure during this interval.

One of the oldest samples from this study, the 703 ± 5 Ma inheritance-rich granodiorite on Wrangel Island, preserves numerous detrital zircons as cores (Fig. 7), signifying that, early on, supracrustal sediments were incorporated in the magmas. Field relationships on Wrangel Island suggest the assimilation of crustal material as late as 620 ± 6 Ma (Fig. 4b), as does the presence of 1.7 Ga zircons in the 574 ± 9 Ma Koolen Lake orthogneiss and 666 ± 5 Ma leucosomes in Koolen Lake paragneiss in far eastern Chukotka (Amato *et al.* 2014).

The three samples of AAC terrane basement analysed here for O isotopes, ranging in age from

661 ± 11 to 574 ± 9 Ma, exhibit mantle-like $\delta^{18}O$ results (Fig. 8). When compared with the global record of O isotopes in zircon since 2 Ga, the results from this study are at the light end of the spectrum, consistent with the limited recycling of high $\delta^{18}O$ sediments (Figs 8 & 11) (Valley 2003). Thus the O isotope results support 661 ± 11 Ma and younger magmatism in a mantle-input dominated system (i.e. a low volume of assimilated material), or the mixing of mantle-derived magmas with crustal materials that had mantle-like O isotope ratios.

The Hf isotopic compositions of the four samples analysed exhibit a near-vertical (i.e. becoming increasingly positive) trend over the time span of the magmatism towards more radiogenic values (Fig. 9), also suggesting an environment with a decreasing input of evolved material during magmatism (Fig. 11). Increasingly radiogenic Hf isotopic compositions of arc crust may indicate the generation of isotopically juvenile mantle-derived melts in a continental arc setting undergoing extension (Mišković & Schaltegger 2009), the subduction-driven removal of arc lithosphere (Collins *et al.* 2011) and/or isolation from evolved sedimentary inputs due to slab retreat and the consequent oceanwards migration of the arc (Collins 2002; Collins & Richards 2008). From a global plate tectonic setting perspective, this trend is characteristic of peripheral orogenic systems (Murphy & Nance 1991), such as the circum-Pacific continental margins since the Mesozoic (Collins *et al.* 2011). As a well-documented example, the geochemical and tectonic evolution of the Tasmanides reflects multiple episodes of juvenile crust formation during the Phanerozoic in a retreating arc tectonic setting (Kemp *et al.* 2009; Collins *et al.* 2011).

Given these similarities, an extensional arc tectonic setting for arc magmatism across the interval 710–580 Ma is supported by the O and Hf isotope geochemistry of zircon and patterns of inheritance over the duration of Neoproterozoic magmatism in the central AAC terrane (Fig. 11). The increasingly juvenile contributions to the bulk composition of the crust suggests that the AAC terrane might have formed as part of a ribbon continent that separated from a larger continental landmass by extension/spreading in an oceanic back-arc region (Fig. 11) (Malone *et al.* 2014). Over the long duration of Neoproterozoic magmatism in the AAC terrane, the geochemical signals of relatively primitive (i.e. mantle-derived, including accreted oceanic crust) v. relatively evolved (i.e. continent-derived) components become progressively more primitive, best exemplified by the steep vertical trend in $\varepsilon Hf_{initial}$ (Fig. 9). The mantle-like isotopic values in zircons as old as 661 ± 11 Ma suggest relatively limited volumes of high $\delta^{18}O$ crust available for assimilation for most of the duration of magmatism, which may indicate that the arc migrated oceanwards early in the time span of magmatism.

Implications

Although it is beyond the intended scope of this paper (the tectono-chemistry of basement rocks in western Chukotka and Wrangel Island), these new data also provide insight into Rodinian continental reconstructions (e.g. Cawood *et al.* 2016) and establish important piercing points for Mesozoic plate tectonic reconstructions of the Arctic (see Miller *et al.* this volume, in press *a*). The peripheral/external fingerprint of Cryogenian–Ediacaran magmatism documented in this study underscores the need to understand the palaeogeographical implications of inheritance in the 703 ± 5 Ma granodiorite and correlative spectra elsewhere in the AAC terrane. Understanding the derivation and crustal sources of these spectra, in conjunction with more comprehensive geochemical and petrological studies of magmatism in the Neoproterozoic basement of the AAC terrane, could better specify the position of the AAC terrane along the margin of Rodinia and elucidate the palaeotectonic relationships between the AAC terrane and the Timanian and Caledonian orogenic belts.

Conclusions

This paper provides new insights into the Neoproterozoic palaeotectonic evolution of the central part of the AAC microplate, for which little data on its basement rock units previously existed. These findings and associated interpretations allow more robust comparisons with displaced terranes and long-lived continental margins in the circum-Arctic region.

(1) Although Cretaceous high-grade metamorphism and deformation have obscured the original lithology of basement rocks in the Velitkenay massif of western Chukotka, integrated zircon U–Pb geochronology, trace element geochemistry and O and Hf isotopic results suggest that the area was a locus of magmatism at 661 ± 11 and 612 ± 7 Ma.

(2) The 661 ± 11 and 612 ± 7 Ma ages from Arctic Chukotka are similar to previously published thermal ionization mass spectrometry ages (Cecile *et al.* 1991). Our newly published SIMS ages for magmatism in the Wrangel Complex on Wrangel Island suggest a shared Neoproterozoic history of the basement complexes in western Chukotka and Wrangel Island.

(3) The inheritance of pre-magmatic zircon is observed at *c.* 700–580 Ma and again at *c.* 100 Ma. This occurs as the incorporation of supracrustal (i.e. detrital) zircons in a 703 ± 5 Ma granodiorite intrusion, as 711 ± 4 Ma granitic xenoliths in 620 ± 6 Ma intrusions and as the inheritance of a population of 612 ± 7 Ma zircons in *c.* 100 Ma leucogranites associated with peak metamorphism in the Velitkenay complex.

(4) The age spectrum of supracrustal zircon inheritance in 703 ± 5 Ma granodiorite from Wrangel Island could have been derived from end-Mesoproterozoic orogen source regions of northern Rodinia (e.g. the Grenville–Sveconorwegian belts) (Fig. 11). These spectra have also been observed in the Brooks Range (Hoiland *et al.* this volume, in press) and rocks mapped as Palaeozoic in the Nome Complex on Seward Peninsula (Till *et al.* 2014*a*, *b*). The similarities and correlation of this detrital zircon signature represent the first evidence of the presence of Neoproterozoic age metasedimentary units within the AAC terrane.

(5) The *c.* 710–580 Ma O–Hf isotopic evolution of zircons from the central AAC terrane crust indicates a temporal trend towards a more primitive magmatic character, consistent with the AAC terrane basement being formed and modified in an 'external' or 'peripheral' orogenic setting (Fig. 11) (Collins *et al.* 2011; Cawood *et al.* 2016).

We are grateful to a number of individuals and institutions for their efforts in assisting our research. Velitkenay massif mapping was aided by G. Polzunenkov and N. Kulik. A. Strickland performed preliminary geochronology work on two of the Wrangel Island samples. Invaluable discussions with numerous Arctic workers about their data were made possible by conference subsidies from CALE. The staff at the Stanford USGS Micro Analysis Center, Nordsim, the UCLA SIMS Laboratory and the WSU Geoanalytical Laboratory are thanked for assistance with analyses and data reduction, and we recognize J. Wooden, M. Coble, M. Whitehouse, R. Economos, J. Vervoort, C. Fisher and C. Knaack for their invaluable guidance. This manuscript benefited greatly from constructive reviews by B. Coakley and an anonymous reviewer. Partial funding of field and laboratory work was provided by multiple grants from CRDF-Global awarded to E. Miller and V. Akinin, a Swedish Research Council grant to V. Pease, RFBR grant 16-05-00949 to V. Akinin and a Stanford School of Earth Sciences McGee grant to E. Gottlieb. The Nordsim facility operates as a joint Nordic infrastructure funded by Denmark, Finland, Norway and Sweden. This is Nordsim publication # 508. This is a CALE contribution. This material is based on work supported by the National Science Foundation under grants NSF-EAR 0948673 and 1624582 (Miller) and 0421795 (UCLA SIMS).

References

Akinin, V.V. & Miller, E.L. 2011. Evolution of calc-alkaline magmas of the Okhotsk-Chukotka Volcanic Belt. *Petrology*, **19**, 237–277.

Akinin, V.V., Miller, E.L. & Wooden, J.L. 2009. Petrology and geochronology of crustal xenoliths from the Bering Strait region: linking deep and shallow processes in extending continental crust. *In*: Miller, R.B. & Snoke, A.W. (eds) *Crustal Cross-Sections from the Western North American Cordillera and Elsewhere: Implications for Tectonic and Petrologic Processes*. Geological Society of America, Special Papers, **456**, 39–68.

Akinin, V.V., Andronikov, A.V., Mukasa, S.B. & Miller, E.L. 2013. Cretaceous lower crust of the continental margins of the northern Pacific: petrologic and geochronologic data on lower to middle crustal xenoliths. *Petrology*, **21**, 28–65, https://doi.org/10.1134/S0869591113010013

Akinin, V.V., Gottlieb, E.S., Miller, E.L., Polzunenkov, G.O., Stolbov, N.M. & Sobolev, N.N. 2015. Age and composition of basement beneath the De Long archipelago, Arctic Russia, based on zircon U–Pb geochronology and O–Hf isotopic systematics from crustal xenoliths in basalts of Zhokhov Island. *Arktos*, **1**, https://doi.org/10.1007/s41063-015-0016-6

Amato, J.M., Toro, J., Miller, E.L., Gehrels, G.E., Farmer, G.L., Gottlieb, E.S. & Till, A.B. 2009. Late Proterozoic–Paleozoic evolution of the Arctic Alaska-Chukotka terrane based on U–Pb igneous and detrital zircon ages: implications for Neoproterozoic paleogeographic reconstructions. *Geological Society of America Bulletin*, **121**, 1219–1235.

Amato, J.M., Aleinikoff, J.N., Akinin, V.V., McClelland, W.C. & Toro, J. 2014. Age, chemistry, and correlations of Neoproterozoic–Devonian igneous rocks of the Arctic Alaska-Chukotka terrane: an overview with new U–Pb ages. *In*: Till, A.B. & Dumoulin, J.A. (eds) *Reconstruction of an Early Paleozoic Continental Margin and its Contained Base Metal Sulfide Deposits: Late Proterozoic to Mississippian Rocks of Seward Peninsula*. Geological Society of America, Special Papers, **506**, 29–57.

Amato, J.M., Toro, J., Akinin, V.V., Hampton, B.A., Salnikov, A.S. & Tuchkova, M.I. 2015. Tectonic evolution of the Mesozoic South Anyui suture zone, eastern Russia: a critical component of paleogeographic reconstructions of the Arctic region. *Geosphere*, **11**, 1530–1564.

Barth, A.P. & Wooden, J.L. 2010. Coupled elemental and isotopic analyses of polygenetic zircons from granitic rocks by ion microprobe, with implications for melt evolution and the sources of granitic magmas. *Chemical Geology*, **277**, 149–159, https://doi.org/10.1016/j.chemgeo.2010.07.017

Bingen, B., Belousova, E.A. & Griffin, W.L. 2011. Neoproterozoic recycling of the Sveconorwegian orogenic belt: detrital-zircon data from the Sparagmite basins in the Scandinavian Caledonides. *Precambrian Research*, **189**, 347–367.

Black, L.P., Kamo, S.L. *et al.* 2004. Improved $^{206}Pb/^{238}U$ microprobe geochronology by the monitoring of a trace-element-related matrix effect: SHRIMP,

ID–TIMS, ELA–ICP–MS and oxygen isotope documentation for a series of zircon standards. *Chemical Geology*, **205**, 115–140.

Bradley, D.C., McClelland, W.C. *et al.* 2014. Proterozoic geochronological links between the Farewell, Kilbuck and Arctic Alaska terranes. *Journal of Geology*, **122**, 237–258.

Brumley, K., Miller, E.L., Konstantinou, A., Meisling, K., Mayer, L. & Wooden, J. 2014. First bedrock samples dredged from outcrops on the Chukchi Borderland, Arctic Ocean. *Geosphere*, https://doi.org/10.1130/GES01044

Cawood, P.A., Nemchin, A.A., Strachan, R., Prave, T. & Krabbendam, M. 2007. Sedimentary basin and detrital zircon record along East Laurentia and Baltica during assembly and breakup of Rodinia. *Journal of the Geological Society, London*, **164**, 257–275.

Cawood, P.A., Strachan, R., Cutts, K., Kinny, P.D., Hand, M. & Pisarevsky, S. 2010. Neoproterozoic orogeny along the margin of Rodinia: Valhalla orogen, North Atlantic. *Geology*, **38**, 99–102.

Cawood, P.A., Strachan, R.A., Pisarevsky, S.A., Gladkochub, D.P. & Murphy, J.B. 2016. Linking collisional and accretionary orogens during Rodinia assembly and breakup: implications for models of supercontinent cycles. *Earth and Planetary Science Letters*, **449**, 118–126.

Cecile, M.P., Harrison, J.C., Kos'ko, M.K. & Parrish, R.R. 1991. Precambrian U–Pb ages of igneous rocks, Wrangel Complex, Wrangel Island USSR. *Canadian Journal of Earth Sciences*, **28**, 1310–1348.

Churkin, M., Jr., & Trexler, J.H., Jr., 1981. Continental plates and accreted oceanic terranes in the Arctic. *In*: Nairn, A.E.M., Churkin, M., Jr., & Stehli, F.G. (eds) *The Arctic Ocean*. Springer, New York, 1–20.

Claiborne, L.L., Miller, C.F. & Wooden, J.L. 2010. Trace element composition of igneous zircon: a thermal and compositional record of the accumulation and evolution of a large silicic batholith, Spirit Mountain, Nevada. *Contributions to Mineralogy and Petrology*, **160**, 511–531, https://doi.org/10.1007/s00410-010-0491-5

Collins, W.J. 2002. Nature of extensional accretionary orogens. *Tectonics*, **21**, 1–12.

Collins, W.J. & Richards, S.W. 2008. Geodynamic significance of S-type granites in circum-Pacific orogens. *Geology*, **36**, 559–562.

Collins, W.J., Belousova, E.A., Kemp, A.I.S. & Murphy, J.B. 2011. Two contrasting Phanerozoic orogenic systems revealed by hafnium isotope data. *Nature Geoscience*, **4**, 333–337, https://doi.org/10.1038/ngeo1127

Ershova, V.B., Prokopiev, A.V. & Khudoley, A.K. 2016. Devonian–Permian sedimentary basins and paleogeography of the Eastern Russian Arctic: an overview. *Tectonophysics*, **691**, 234–255.

Fisher, C.M., Vervoort, J.D. & DuFrane, S.A. 2014. Accurate Hf isotope determinations of complex zircons using the 'laser ablation split stream' method. *Geophysics, Geochemistry, Geosystems*, **15**, https://doi.org/10.1002/2013GC004962

Franke, D., Reichert, C., Damm, V. & Piepjohn, K. 2008. The South Anyui suture, northeast Arctic Russia, revealed by offshore seismic data. *Norwegian Journal of Geology*, **88**, 189–200.

Gehrels, G. 2010*a*. Normalized age probability plots: Arizona LaserChron Center, http://sites.google.com/a/laserchron.org/laserchron/ [last accessed December 2013].

Gehrels, G. 2010*b*. Cumulative age probability plots: Arizona LaserChron Center; http://sites.google.com/a/laserchron.org/laserchron/ [last accessed December 2013].

Grantz, A., Clark, D.L., Phillips, R.L. & Srivastava, S.P. 1998. Phanerozoic stratigraphy of Northwind Ridge, magnetic anomalies in the Canada Basin, and the geometry and timing of rifting in the Amerasia Basin, Arctic Ocean. *Geological Society of America Bulletin*, **110**, 801–820.

Hanchar, J.M. & Miller, C.F. 1993. Zircon zonation patterns as revealed by cathodoluminescence and backscattered electron images: implications for interpretation of complex crustal histories. *Chemical Geology*, **110**, 1–13.

Hannula, K.A., Miller, E.L., Dumitru, T.A., Lee, J. & Rubin, C.M. 1995. Structural and metamorphic relations in the southwest Seward Peninsula, Alaska: crustal extension and the unroofing of blueschists. *Geological Society of America Bulletin*, **107**, 536–553, https://doi.org/10.1130/0016-7606(1995)107<0536:SAMRIT>2.3.CO;2

Hoiland, C.H., Miller, E.L., Pease, V., Hourigan, J.K. In press. Detrital zircon U-Pb geochronology and Hf isotope geochemistry of metasedimentary strata in the southern Brooks Range: Constraints on Neoproterozoic–Cretaceous evolution of Arctic Alaska. *In*: Pease, V. & Coakley, B. (eds) *Circum Arctic Lithosphere Evolution*. Geological Society, London, Special Publications, **460**, https://doi.org/10.1144/SP460.16

Hoskin, P.W.O. & Schaltegger, U. 2003. The composition of zircon and igneous and metamorphic petrogenesis. *Reviews in Mineralogy and Geochemistry*, **53**, 27–62.

Hourigan, J.K., Brandon, M.T., Soloviev, A.V., Kirmasov, A.B., Garver, J.I., Stevenson, J. & Reiners, P.W. 2009. Eocene arc-continent collision and crustal consolidation in Kamchatka, Russian Far East. *American Journal of Science*, **309**, 333–396.

Ireland, T.R. & Williams, I.S. 2003. Considerations in zircon geochronology by SIMS. *Reviews in Mineralogy and Geochemistry*, **53**, 215–241.

Jakobsson, M., Mayer, L.A. *et al.* 2012. The international bathymetric chart of the Arctic Ocean (IBCAO) version 3.0. *Geophysical Research Letters*, **39**, https://doi.org/10.1029/2012GL052219

Karl, S.M. & Aleinikoff, J.N. 1990. Proterozoic U–Pb zircon age of granite in the Kallarichuk Hills, western Brooks Range Alaska: evidence for Precambrian basement in the schist belt. *In*: Dover, J.H. & Galloway, J.P. (eds) *Geologic Studies in Alaska by the US Geological Survey, 1989. US Geological Survey Bulletin*, **1946**, 95–100.

Kemp, A.I.S., Hawkesworth, C.J., Collins, W.J., Cray, C.M. & Blevin, P.L. 2009. Isotopic evidence for rapid continental growth in an extensional accretionary orogen: the Tasmanides, eastern Australia. *Earth and Planetary Science Letters*, **284**, 455–466.

Kirkland, C.L., Daly, J.S. & Whitehouse, M.J. 2006. Granitic magmatism of Grenvillian and late

Neoproterozoic age in Finnmark, arctic Norway: constraining pre-Scandian deformation in the Kalak Nappe Complex. *Precambrian Research*, **145**, 24–52.

KIRKLAND, C.L., DALY, J.S. & WHITEHOUSE, M.J. 2007. Provenance and terrane evolution of the Kalak Nappe Complex, Norwegian Caledonides: implications for Neoproterozoic paleogeography and tectonics. *Journal of Geology*, **115**, 21–41.

KIRKLAND, C.L., BINGEN, B., WHITEHOUSE, M.J., BEYER, E. & GRIFFIN, W.L. 2011. Neoproterozoic palaeogeography in the North Atlantic Region: inferences from the Akkajaure and Seve Nappes of the Scandinavian Caledonides. *Precambrian Research*, **186**, 127–146.

KLEMPERER, S.L., MILLER, E.L., GRANTZ, A., SCHOLL, D.W. & BERING-CHUKCHI WORKING GROUP 2002. Crustal structure of the Bering and Chukchi shelves: deep seismic reflection profiles across the North American continent between Alaska and Russia. *In*: MILLER, E.L., GRANTZ, A. & KLEMPERER, S.L. (eds) *Tectonic Evolution of the Bering Shelf–Chukchi Sea–Arctic Margin and Adjacent Landmasses*. Geological Society of America, Special Papers, **360**, 1–24.

KOS'KO, M.K., LOPATIN, B.G. & GANELIN, V.G. 1990. Major geological features of the islands of the east Siberian and Chukchi seas and northern coast of Chukotka. *Marine Geology*, **93**, 349–367.

KOS'KO, M.K., CECILE, M.P., HARRISON, J.C., GANELIN, V.G., KHANDOSHKO, N.V. & LOPATIN, B.G. 1993. Geology of Wrangel Island, between Chukchi and East Siberian seas, northeastern Russia. *Geological Survey of Canada Bulletin*, **461**, 1–107.

KRÖNER, A. 2010. The role of geochronology in understanding continental evolution. *In*: KUSKY, T., ZHAI, M.-G. & XIAO, W. (eds) *The Evolving Continents: Understanding Processes of Continental Growth*. Geological Society, London, Special Publications, **338**, 179–196.

KUZMICHEV, A.B. 2009. Where does the South Anyui suture go in the New Siberian islands and Laptev Sea? Implications for the Amerasia basin origin. *Tectonophysics*, **463**, 86–108.

LANE, L.S., CECILE, M.P., GEHRELS, G.E., KOS'KO, M.K., LAYER, P.W. & PARRISH, R.R. 2015. Geochronology and structural setting of Latest Devonian–Early Carboniferous magmatic rocks, Cape Kiber, northeast Russia. *Canadian Journal of Earth Sciences*, **52**, 147–160.

LUDWIG, K.R. 2009. *SQUID 2: A user's manual, rev. 12 Apr. 2009*. Berkeley Geochronology Center, Special Publication, **5**, 110 p.

LUDWIG, K.R. 2012. *Isoplot, A Geochronological Toolkit for Microsoft Excel*. Berkeley Geochronology Center, Special Publications, **5**.

MALONE, S.J. 2012. *Tectonic evolution of northern Ellesmere Island: insights from the Pearya Terrane, Ellesmerian Clastic Wedge and Sverdrup Basin*. PhD thesis, University of Iowa.

MALONE, S.J., MCCLELLAND, W.C., VON GOSEN, W. & PIEPJOHN, K. 2014. Proterozoic evolution of the North Atlantic–Arctic Caledonides: insights from detrital zircon analysis of metasedimentary rocks from the Pearya Terrane, Canadian High Arctic. *Journal of Geology*, **122**, 623–648.

MARELLO, L., EBBING, J. & GERNIGON, L. 2013. Basement inhomogeneities and crustal setting in the Barents Sea from a combined 3D gravity and magnetic model. *Geophysical Journal International*, https://doi.org/10.1093/gji/ggt018

MILLER, E.L. & HUDSON, T.C. 1991. Mid-Cretaceous extensional fragmentation of a Jurassic–Early Cretaceous compressional orogen, Alaska. *Tectonics*, **10**, 781–796, https://doi.org/10.1029/91TC00044

MILLER, E.L. & VERZHBITSKY, V.E. 2009. Structural studies near Pevek, Russia: implications for formation of the East Siberian Shelf and Makarov Basin of the Arctic Ocean. *In*: STONE, D.B., FUJITA, K., LAYER, P.L., MILLER, E.L., PROKOPIEV, A.V. & TORO, J. (eds) *Geology, Geophysics and Tectonics of Northeastern Russia: a Tribute to Leonid Parfenov*. European Geosciences Union, Stephan Mueller Special Publication Series, **4**. Copernicus, Göttingen, 223–241.

MILLER, E.L., CALVERT, A.T. & LITTLE, T.A. 1992. Strain-collapsed metamorphic isograds in a sillimanite gneiss dome, Seward Peninsula, Alaska. *Geology*, **20**, 487–490.

MILLER, E.L., KATKOV, S.M., STRICKLAND, A., TORO, J., AKININ, V.V. & DUMITRU, T.A. 2009. Geochronology and thermochronology of Cretaceous plutons and metamorphic country rocks, Anyui-Chukotka fold belt, North East Arctic Russia. *In*: STONE, D.B., FUJITA, K., LAYER, P.L., MILLER, E.L., PROKOPIEV, A.V. & TORO, J. (eds) *Geology, Geophysics and Tectonics of Northeastern Russia: a Tribute to Leonid Parfenov*. European Geosciences Union, Stephan Mueller Special Publication Series, **4**. Copernicus, Göttingen, 157–175.

MILLER, E.L., GEHRELS, G.E., PEASE, V. & SOKOLOV, S. 2010. Stratigraphy and U–Pb detrital zircon geochronology of Wrangel Island, Russia: implications for Arctic paleogeography. *American Association of Petroleum Geologists Bulletin*, **94**, 665–692.

MILLER, E.L., MEISLING, K.E. *ET AL*. In press a. Circum-Arctic Lithosphere Evolution (CALE) Transect C: displacement of the Arctic Alaska–Chukotka microplate toward the Pacific during opening of the Amerasia Basin of the Arctic. *In*: PEASE, V. & COAKLEY, B. (eds) *Circum Arctic Lithosphere Evolution*. Geological Society, London, Special Publications, **460**, https://doi.org/10.1144/SP460.9

MILLER, E.L., AKININ, V.V., DUMITRU, T., GOTTLIEB, E., GROVE, M., MEISLING, K. & SEWARD, G. In press b. Deformational history and thermochronology of Wrangel Island, East Siberian shelf, and coastal chukotka, Arctic Russia. *In*: PEASE, V. & COAKLEY, B. (eds) *Circum Arctic Lithosphere Evolution*. Geological Society, London, Special Publications, **460**, https://doi.org/10.1144/SP460.7

MIŠKOVIĆ, A. & SCHALTEGGER, U. 2009. Crustal growth along a non-collisional cratonic margin: a Lu–Hf isotopic survey of the Eastern Cordilleran granitoids of Peru. *Earth and Planetary Science Letters*, **279**, 303–315.

MOORE, T.E., WALLACE, W.K., BIRD, K.J., KARL, S.M., MULL, C.G. & DILLON, J.T. 1994. Geology of northern Alaska. *In*: PLAFKER, G. & BERG, H.C. (eds) *The Geology of Alaska*. Geological Society of America, Geology of North America Series, **G-1**, 49–140.

MURPHY, J.B. & NANCE, R.D. 1991. Supercontinent model for the contrasting character of Late Proterozoic orogenic belts. *Geology*, **19**, 469–472.

NATAL'IN, B.A., AMATO, J.M. & TORO, J. 1999. Paleozoic rocks of northern Chukotka Peninsula: implications for the tectonics of the Arctic region. *Tectonics*, **18**, 977–1003.

NOKLEBERG, W.J., PARFENOV, L.M. *ET AL.* 2000. *Phanerozoic Tectonic Evolution of the Circum-North Pacific*. US Geological Survey, Professional Papers, **1626**, 1–122.

PATRICK, B.E. 1988. Synmetamorphic structural evolution of the Seward Peninsula blueschist terrane, Alaska. *Journal of Structural Geology*, **10**, 555–565.

PATRICK, B.E. & MCCLELLAND, W.C. 1995. Late Proterozoic granitic magmatism on Seward Peninsula and a Barentian origin for Arctic Alaska–Chukotka. *Geology*, **23**, 81–84.

PEASE, V., DRACHEV, S., STEPHENSON, R. & ZHANG, X. 2014. Arctic lithosphere: a review. *Tectonophysics*, **628**, 1–25.

PETTERSSON, C.H., TEBENKOV, A.M., LARIONOV, A.N., ANDRESEN, A. & PEASE, V. 2009. Timing of migmatization and granite genesis in the Northwestern Terrane of Svalbard, Norway: implications for regional correlations in the Arctic Caledonides. *Journal of the Geological Society, London*, **166**, 147–158, https://doi.org/10.1144/0016-76492008-023

SIRCOMBE, K.N. 2007. Mountains in the shadows of time: three-dimensional density distribution mapping of U–Pb isotopic data as a visualization aid for geochronological information in concordia diagrams. *Geochemistry, Geophysics, Geosystems*, **7**, Q07013, https://doi.org/10.1029/2005GC001052

SPENCER, C.J., CAWOOD, P.A., HAWKESWORTH, C.J., PRAVE, A.R., ROBERTS, N.M.W., HORSTWOOD, M.S.A. & WHITEHOUSE, M.J. 2015. Generation and preservation of continental crust in the Grenville orogeny. *Geoscience Frontiers*, **6**, 357–372.

STACEY, J.S. & KRAMERS, J.D. 1975. Approximation of terrestrial lead isotope evolution by a two-stage model. *Earth and Planetary Science Letters*, **26**, 207–221.

TIKHOMIROV, P.L., KALININA, E.A., KOBAYASHI, K. & NAKAMURA, E. 2008. Late Mesozoic silicic magmatism of the North Chukotka area (NE Russia): age, magma sources, and geodynamic implications. *Lithos*, **105**, 329–346.

TILL, A.B., SCHMIDT, J.S. & NELSON, S.W. 1988. Thrust involvement of metamorphic rocks, southwestern Brooks Range, Alaska. *Geology*, **16**, 930–933.

TILL, A.B., DUMOULIN, J.A., AYUSO, R.A., ALEINIKOFF, J.N., AMATO, J.M., SLACK, J.F. & SHANKS, W.C., III. 2014*a*. *Reconstruction of an Early Paleozoic Continental Margin Based on the Nature of Protoliths in the Nome Complex, Seward Peninsula, Alaska*. Geological Society of America, Special Papers, **506**, 1–28.

TILL, A.B., AMATO, J.M., ALEINIKOFF, J.N. & BLEICK, H.A. 2014*b*. *U–Pb Detrital Zircon Geochronology as Evidence for the Origin of the Nome Complex, Northern Alaska, and Implications for Regional and Trans-Arctic Correlations*. Geological Society of America, Special Papers, **506**, 111–131.

TRAIL, D., MOJZSIS, S.J., HARRISON, T.M., SCHMITT, A.K., WATSON, E.B. & YOUNG, E.D. 2007. Constraints on Hadean zircon protoliths from oxygen isotopes, Ti-thermometry, and rare earth elements. *Geochemistry, Geophysics, Geosystems*, **8**, Q06014, https://doi.org/10.1029/2006GC001449

VALLEY, J.W. 2003. Oxygen isotopes in zircon. *Reviews in Mineralogy and Geochemisty*, **53,** 343–386.

VERNIKOVSKY, V.A., METELKIN, D.V., VERNIKOVSKAYA, A.E., SAL'NIKOVA, E.B., KOVACH, V.P. & KOTOV, A.B. 2011. The oldest island arc complex of Taimyr: concerning the issue of the Central-Taimyr accretionary belt formation and paleogeodynamic reconstructions in the arctic. *Doklady Earth Sciences*, **436**, 186–192, https://doi.org/10.1134/S1028334X1102019X

VERVOORT, J.D. & BILCHERT-TOFT, J. 1999. Evolution of the depleted mantle: Hf isotope evidence from juvenile rocks through time. *Geochimica et Cosmochimica Acta*, **63**, 533–556.

VERVOORT, J.D. & PATCHETT, P.J. 1996. Behavior of hafnium and neodymium isotopes in the crust: constraints from Precambrian crustally derived granites. *Geochimica et Cosmochimica Acta*, **251**, 3717–3733.

WIEDENBECK, M., ALLÉ, P. *ET AL.* 1995. Three natural zircon standards for U–Th–Pb, Lu–Hf, trace element and REE analyses. *Geostandards Newsletter*, **19**, 1–23.

WIEDENBECK, M., HANCHAR, J.M. *ET AL.* 2004. Further characterisation of the 91500 zircon crystal. *Geostandards and Geoanalytical Research*, **28**, 9–39.

WHITEHOUSE, M.J. & KAMBER, B.S. 2005. Assigning dates to thin gneissic veins in high-grade metamorphic terranes – a cautionary tale from Akilia, southwest Greenland. *Journal of Petrology*, **46**, 291–318.

WHITEHOUSE, M.J., KAMBER, B.S. & MOORBATH, S. 1999. Age significance of U–Th–Pb zircon data from Early Archaean rocks of west Greenland: a reassessment based on combined ion-microprobe and imaging studies. *Chemical Geology*, **160**, 201–224.

ZHANG, W., ROBERTS, D. & PEASE, V. 2015. Age provenance characteristics and regional implications of Neoproterozoic, Timanian–margin successions and a basal Caledonian nappe in northern Norway. *Precambrian Research*, **268**, 153–167.